Understanding the Physiological Functions of the Host Xenobiotic-sensing Nuclear Receptors PXR and CAR on the Gut Microbiome using Genetically-modified Mice

Mallory Little

A thesis submitted in partial fulfillment of the requirements for the degree of

Master of Public Health

University of Washington

2019

Committee:

Julia Yue Cui

Elaine Faustman

Program Authorized to Offer Degree:

Department of Environmental and Occupational Health Sciences

University of Washington

ABSTRACT

Understanding the Physiological Functions of the Host Xenobiotic-sensing Nuclear Receptors PXR and CAR on the Gut Microbiome using Genetically-modified Mice

Mallory Little

Chair of the Supervisory Committee:

Dr. Julia Yue Cui

Department of Environmental & Occupational Health Sciences

The pregnane X receptor (PXR) and constitutive androstane receptor (CAR) are important xenobiotic-sensing nuclear receptors, and their genetic polymorphisms are known to alter the pharmacokinetics of various xenobiotics. The gut microbiome is increasingly recognized as a critical modifier of host xenobiotic biotransformation, and microbial metabolites such as lithocholic acid and indole-3-propionic acid are known endogenous PXR activators. We have previously demonstrated that the gut microbiome is necessary for maintaining the constitutive expression of certain PXR- and CAR-target genes, and pharmacological activation of PXR and CAR produces gut dysbiosis and reduces secondary bile acids. However, little is known regarding to what extent PXR and CAR under basal conditions influence the gut microbiome. To fill this knowledge gap, we examined the gut microbiome compositions under three different settings: 1) two mouse strains that express different basal levels of PXR and CAR (C57BL/6J that expresses lower PXR and CAR vs FVB/NJ that expresses higher PXR and CAR); 2) wild type (WT), PXR-null, CAR-null, and PXR-CAR-double null mice; and 3) mice that carry either mouse (m) or human (h) PXR genes. 24h fecal samples were collected from these mice at

adolescent (30-day-old) and adult (60-day-old) ages of both genders. 16S rDNA sequencing was performed by amplifying the hypervariable V4 region (n=5 per group). Compared to C57BL/6J mice, FVB/NJ mice had higher richness in gut microbiome in both ages and genders, and had higher percentages of certain pro-inflammatory bacteria. This correlated with higher pro-inflammatory cytokines in feces of FVB/NJ mice (cytokine array). The absence of PXR or CAR markedly increased the richness of gut microbiome, and the absence of both receptors had the highest richness of gut microbiome of both ages and genders. Most notably, the PXR-CAR-double null mice had higher percentages of the *Lactobacillus* genus, which is known to carry bile salt hydrolase (BSH) activities, and this corresponded to a decrease in most taurine conjugated bile acids (BAs) in feces (LC-MS). PXR-CAR-double null mice also had higher acetic acid in feces of adolescent males, and C10 in feces of adult males (GC-MS). Compared to WT mice that carry mPXR, hPXR-transgenic (TG) mice had higher *Prevotella* genus. In addition, there was an apparent increase in several unconjugated 12-OH BAs as well as ursodeoxycholic acid (UDCA), but an apparent decrease in several 6-OH BAs, in feces of hPXR-TG mice. hPXR-TG mice also had higher propionic acid in males, as well as lower 2-methylbutyric acid in both genders. In conclusion, the present study is among the first to show that the host genotypes of the major xenobiotic-sensing nuclear receptors PXR and CAR profoundly influence the composition and metabolites of the gut microbiome, and the basal levels of PXR and CAR may act through gut microbiome to modulate host diseases such as inflammation and metabolic syndrome.

INTRODUCTION

The gut microbiome is a community comprised of bacteria, archaea, viruses, protozoa, and fungi in the human gastrointestinal system. Current estimates place the bacteria to human cell ratio (B/H) at 1.3 (Sender et al., 2016). The composition of the gut microbiome varies greatly among individuals and is affected by factors such as host genetics, diet, age, exercise, medication, disease status, birth process, stress, and location in the world (Cresci and Bawden, 2015; Luca et al., 2018). The composition of the gut microbiome also varies within an individual according to location along the gastrointestinal tract, correlating with pH (Seekatz et al., 2019).

The gut microbiome has a variety of effects on host metabolism. Regarding intermediary metabolism, the gut microbiome aids in digestion by fermenting carbohydrates to produce short-chain fatty acids (SCFAs) such as acetate, butyrate, and propionate. SCFAs are used as energy sources for colonocytes and protect against colitis by regulating regulatory T (Treg) cells as well as through other anti-inflammatory functions (Smith et al., 2013). The gut microbiome also modulates glucose homeostasis; for example, *Akkermansia (A.) muciniphila* is associated

with restoring insulin sensitivity in high-fat diet fed animals by increasing glucagon like peptide 1 (GLP-1), an intestinal incretin (Martinez et al., 2016). Intestinal bacteria can deconjugate and reduce host-derived primary bile acids (BAs) into secondary BAs via the microbial enzymes bile salt hydrolase and bile acid 7α-dehydroxylase (Ridlon et al., 2014). Certain secondary BAs are more potent activators of the host Takeda G-protein-coupled receptor 5 (TGR5) than primary BAs, and this can promote thermogenesis and energy expenditure of the host (Watanabe et al., 2006). At exceedingly high concentrations, secondary BAs are considered more toxic than primary BAs, and are implicated in cholestatic liver injury, inflammation, and cancer (Li and Apte, 2015).

Regarding xenobiotic metabolism, the gut microbiome can utilize their enzymes to directly biotransform chemicals. For example, *Eggerthella lenta* contains cardiac glycoside operons (Cprs) that inactivate the cardiac glycoside digoxin (Lindenbaum et al., 1981). Another example is that co-administration of the antibiotic rifaximin with non-steroidal anti-inflammatory drugs (NSAIDs) ameliorates bacteria-induced enteropathy (Scarpignato et al., 2017). The gut microbiome can also modulate host xenobiotic metabolism through indirect mechanisms. For example, the absence of gut microbiota in mice alters the expression of xenobiotic-processing genes, such as those for cytochrome P450 enzymes and other phase I oxidases(Fu et al., 2017). The absence of gut microbiota in mice alters the host metabolism of polybrominated diphenyl ethers (PBDEs), resulting in different levels of PBDE metabolites compared to conventional mice, and modulates the PBDE-mediated differential regulation of xenobiotic-processing genes (Li et al., 2017a). Therefore, a personalized treatment regimen is sometimes necessary depending on gut microbial composition.

The pregnane X receptor (PXR) and constitutive androstane receptor (CAR) are two major xenobiotic-sensing nuclear receptors of the host, and they are highly expressed in liver and intestine. Upon ligand activation, PXR and CAR up-regulate certain drug-metabolizing

enzymes and efflux transporters as a compensatory mechanism against xenobiotic insult (Aleksunes and Klaassen, 2012; Oladimeji and Chen, 2018). PXR and CAR share many target genes such as the drug-metabolizing enzyme CYP3A4 in humans (Banerjee et al., 2015). However, there are known differences between PXR and CAR. For example, CAR is constitutively active and so it activates target genes even in the absence of an exogenous ligand, distinguishing itself from PXR (Oladimeji and Chen, 2018). For example, CAR is indirectly activated by the central nervous system depressant phenobarbital due to an epidermal growth factor-mediated mechanism leading to its activation via dephosphorylation (Mutoh et al., 2013).

PXR and CAR are known as promiscuous nuclear receptors because a wide variety of ligands can attach to their ligand-binding domains and induce gene transcription (Watkins et al., 2001). For pharmaceuticals, for example, PXR and CAR are both activated by the antifungal voriconazole and coordinate in its metabolism (Ohbuchi et al., 2013). PXR and CAR are also activated by environmental chemicals such as specific congeners of the PBDE flame retardants and non-coplanar polychlorinated biphenyls (PCBs) (Li et al., 2018; Pencikova et al., 2018). In addition to environmental chemicals and pharmaceuticals, PXR and CAR can be activated by endogenous ligands such as steroids and BAs (Zhou and Hylemon, 2014). PXR and CAR are also activated by a number of herbal remedies, and are involved in drug-drug and drug-food interactions as well as human diseases such as inflammatory bowel disease (IBD) and cholestasis (Xu et al., 2016). A wide variety of bacterial metabolites in the colonic lumen activate PXR and CAR, such as the tryptophan metabolite indole-3-propionic acid (IPA) and the secondary BAs deoxycholic acid (DCA) and lithocholic acid (LCA) (Bhutia et al., 2017). It is theorized that these metabolites are able to bind to these nuclear receptors (Sivaprakasam et al., 2017). In livers of germ-free mice (GF), the prototypical PXR-target genes Cyp3a11 and Cyp3a44 were down-regulated compared to mice with normal intestinal microbiota (CV). This

purportedly occurs because of decreased PXR-activation due to decreased microbial metabolite PXR ligands, however, this same study reports an increase in the mRNA of all transcription factors in livers of GF mice (Selwyn et al., 2015). This relationship has been explored in another paper where specific-pathogen free (SPF) mice had higher cytochrome P450 isozyme expression with accompanying higher PXR and CAR expression than GF mice, due to increased LCA (Toda et al., 2009). Therefore, the presence of the gut microbiome affects the expression of PXR- and CAR-target genes as well as the receptors themselves, as well as the activity of PXR and CAR through modulating their activators.

PXR and CAR are important for human diseases in addition to their well-established adverse effects due to drug-drug interactions. For example, PXR has been shown to play an anti-inflammatory role in the prevention of IBD by inhibiting the NF-κB transcription factor (Shah et al., 2007) as well as NF-κB targeted pro-inflammatory response genes (Xu et al., 2016). The activation of PXR via the microbial metabolite IPA, which is produced from *Clostridium sporogenes,* decreases intestinal permeability and maintains the gut barrier functions (Zhou and Hylemon, 2014). PXR activation also inhibits inflammation through inhibiting the toll-like receptor 4 (TLR4) pathway, thus preventing the overproduction of cytokines. This is supported by the observation that PXR-null mice are more susceptible to *Listeria monocytogenes* infection (Qiu et al., 2016). PXR inhibits the TLR4 pathway by decreasing the stability of TLR4 mRNA and may also repress TLR4 gene transcription (Ranhotra et al., 2016). This TLR4 upregulation due to PXR deficiency can also cause a leaky gut physiology (Venkatesh et al., 2014), which can be resolved by PXR activation via microbial metabolites as previously described (Ma et al., 2018). At the transcriptional level, it has been suggested that the anti-inflammatory SCFA butyrate increases the transcription of PXR (Ranhotra et al., 2016). Additionally, PXR has been recognized for its role in energy homeostasis and glucose metabolism and is correlated with obesity (He et al., 2013). Interestingly, CAR is negatively correlated with obesity, and has been

shown to improve insulin sensitivity (Gao et al., 2009). Activation of CAR by environmental chemicals has been shown to cause health effects such as rodent liver tumor formation, non-alcoholic fatty liver disease, as well as drug-interactions due to the up-regulation of cyp3a enzymes (Ihunnah et al., 2011; Ranhotra et al., 2016). Polymorphisms can affect the function of PXR and CAR as well; for example, a single-nucleotide polymorphism (SNP) in PXR decreases risk for anti-tuberculosis drug-induced hepatotoxicity (Wang et al., 2019).

Species differences in PXR and CAR genetic sequences have also been shown to affect function due to substitutions at ligand-contacting residues (Kublbeck et al., 2016). The most characterized example of this is the mouse-specific PXR-agonist PCN, and the human-specific PXR-agonist rifampicin (LeCluyse, 2001), as well as the mouse-specific CAR-agonist TCPOBOP, and the human-specific CAR-agonist CITCO (Zhang et al., 2013; Park et al., 2016; de Boussac et al., 2018). Activation of CAR leads to tumor formation in liver of mice but not in humans(Elcombe et al., 2014). However, species-selective PXR activators do produce liver enlargement and accelerate regeneration in both wild type (WT) and humanized PXR transgenic (hPXR-TG) mice, as mediated by induced nuclear translocation of yes-associated protein (YAP) (Jiang et al., 2019).

Pharmacological and toxicological exposures can affect the composition of the gut microbiome. Treatment with the NSAID indomethacin caused an increase in bacteria in the S24-7 family compared to co-treatment with the microbial metabolite indole, which caused an increase in members of the Clostridiales order instead. Notably, co-treatment with indole reduced inflammation and intestinal mucosal damage (Whitfield-Cargile et al., 2016), possibly through a PXR-mediated mechanism. Indeed, IPA activates PXR, leading to the down-regulation of the TLR pathway and pro-inflammatory tumor necrosis factor α (TNFα) (Venkatesh et al., 2014). In another study, mice treated with statins resulted in weight gain, increased members of the S24-7 family, up-regulation of PXR-target genes, reduced butyrate, and

increased DCA (Caparros-Martin et al., 2017). After repeating this experiment in PXR-null mice, it was determined that these effects of statins were PXR-dependent. In mice, pharmacological activation of PXR and CAR by their prototypical ligands PCN and TCPOBOP affects the composition of the gut microbiome by down-regulating certain BA-metabolizing bacteria in the intestine(Dempsey et al., 2019). In another study, mice orally-gavaged with PBDEs, which are PXR and CAR activators, had increased *A. muciniphila* and Erysipelotrichaceae *Allobaculum* spp., as well as unconjugated secondary BAs (Li et al., 2018). In another study, mice dosed with polychlorinated biphenyls (PCBs), which can also activate PXR and CAR, had increased *A. muciniphila*, *Clostridium scindens*, *Enterococcus* sp., and *Prevotella* sp. as well as serum BAs (Cheng et al., 2018). In summary, pharmacological and toxicological activation of PXR and CAR can alter the composition of the gut microbiome and the production of distinct microbial metabolites.

While a wealth of literature has demonstrated evidence that the gut microbiome affects PXR and CAR through microbial metabolites, and that pharmacological and toxicological PXR activation affects the composition of the gut microbiome, no studies have been conducted examining the physiological functions PXR and CAR on the gut microbiome. Therefore, this study aims to characterize this potential relationship.

MATERIALS AND METHODS

***Chemicals and reagents*.** E.Z.N.A.® Genomic DNA Isolation Kits were purchased from Omega Bio-Tek (Norcross, GA). The following deuterated internal standards (IS) were used: d4-DCA (CDN Isotopes; CAS No: 112076-61-6), d4-GCA (CDN Isotopes; CAS No: 1201918-15-1), d4-CDCA (CDN Isotopes; CAS No: 99102-69-9), d4-CA (TRC, Canada; Cat no #: C432603), d4-GCDCA (Iso Sciences, CAS No: 1201918-16-2), lithocholic acid-2,2,4,4-D4 (LCA-D4) (PubChem CID of LCA: 9903, Steraloids). 19 major BAs were quantified, namely taurine-conjugated cholic acid (T-CA), T- α muricholic acid (T- α MCA), T- β MCA, T- ω MCA, T-

chenodeoxycholic acid (T-CDCA), T-ursodeoxycholic acid (T-UDCA), T-hyodeoxycholic acid (T-HDCA), T-deoxycholic acid (T-DCA), T-lithocholic acid (T-LCA), α MCA, β MCA, CA, CDCA, UDCA, ω MCA, MDCA, HDCA, DCA, and LCA. CA, CDCA, DCA, and LCA were purchased from Sigma Aldrich (St. Louis, Missouri); α MCA, β MCA were purchased from Steraloids (Newport, Rhode Island). ω MCA and T-ωMCA was a kind gift from Dr. Daniel Raftery's laboratory at University of Washington Northwest Metabolomics Research Center. Other BAs were kindly obtained from University of Kansas Medical Center. Agilent ZORBAX Eclipse Plus C18 columns were purchased from Waters Corporation (Milford, Massachusetts). The samples were eluted using gradient mobile phases of A (10 mM ammonium acetate in 20% acetonitrile) and B (10 mM ammonium acetate in 80% acetonitrile). The UPLC/MS-MS operating parameters are shown in Supplemental Table 1. All other chemicals and reagents, unless indicated otherwise, were purchased from Sigma-Aldrich (St. Louis, MO).

Animals. C57BL/6J wild-type (WT) breeders were purchased from the Jackson Laboratory (Bar Harbor, ME) and then bred in-house (n=5, both genders). PXR-null mice were generated and backcrossed into C57BL/6J background as described previously (Staudinger et al., 2001), and pups were obtained from in-house breeders (n=5 per group). CAR-null mice in C57BL/6J background were generated by Tularik Inc. (South San Francisco, CA) as described previously(Ueda et al., 2002), obtained from University of Kansas Medical Center (Kansas City, KS), and pups were obtained from in-house breeders (n=5 per group). PXR-CAR-null male and female mice in C57BL/6J background were generated by crossing PXR-null and CAR-null mice (n=5). FVB/NJ WT male and female mice were purchased from the Jackson Laboratory (aged 21 days upon arrival, n=5), and were acclimated for at least 9 days within the animal facilities prior to experiments. Male and female humanized PXR (hPXR) breeders in the FVB/NJ background were a generous gift from Frank Gonzalez (National Cancer Institute, Bethesda, MD) and were bred in-house (n=5). All mice were individually housed at weaning age (28 days

old for C57BL/6J mice, due to the significantly small size of the CAR-null mice; and 21 days old for FVB/NJ mice) in the animal facility at the University of Washington according to the Association for Assessment and Accreditation of Laboratory Animal Care International guidelines (https://aaalac.org/resources/theguide.cfm). All mice were exposed to laboratory autoclaved rodent diet (LabDiet #5010, LabDiet, St. Louis, MO), non-acidified autoclaved water, and autoclaved Enrich-N'Pure bedding (Andersons, Maumee, OH). All studies were approved by the Institutional Animal Care and Use Committee at the University of Washington. 24-hour fecal samples were collected from mice at adolescent age (30-days of age) and adult age (60-74 days of age).

DNA isolation. Total DNA was isolated from frozen fecal samples using E.Z.N.A.® Genomic DNA Isolation Kits (Omega Bio-Tek, Norcross, GA) according to the manufacturer's protocol, and the concentration was quantified using a Qubit fluorometer (Thermo Fisher Scientific, Waltham, MA). The 16S rDNA sequencing was performed by Novogene Corporation (Sacramento, CA, 250bp paired-end, n=5 per group).

BA quantification. Approximately 50 mg of fecal samples were homogenized in 1 mL of H_2O. 10 µl of IS was added to 200 µl of fecal sample homogenate, mixed, and equilibrated on ice for 5-10 minutes. 1.5 ml of ice-cold alkaline acetonitrile (5% ammonia in acetonitrile) was added to the homogenate, which was then vortexed vigorously and shaken continuously for 1 hour at room temperature. The mixture was then centrifuged at 12,000 *g* for 15 minutes at 4 °C, and the supernatant was collected into 5 mL glass tubes. The pellet was resuspended in 750 uL of 100% methanol, shaken for 20 minutes, and centrifuged at 15,000 *g* for 20 minutes. The two supernatants obtained were combined, evaporated under vacuum (45 °C) for 4 hours, and reconstituted in 100 µl of 50% methanol. The suspension was transferred into a 0.2 µm Costar Spin-X HPLC microcentrifuge filter (purchased from Corning Inc., Corning, NY), and centrifuged

at 12,000 *g* for 10 minutes. 19 BAs were quantified using liquid chromatography–tandem mass spectrometry (LC-MS/MS).

SCFA quantification*.* The SCFA extraction procedures were performed under 4 ^{o}C. Each fecal sample (20 mg) was mixed with 20 µL aqueous solution of NaOH (0.5 M), 20 µL internal standard solution (hexanoic acid-6,6,6-d_3; 200 µM), and 460 µL MeOH in an Eppendorf tube (1.5 mL). After homogenization (2 min), 400 µL MeOH and 100 µL water were added into the tube. The pH value for the mixture was adjusted to 9. Then the sample was vortexed for 30 s, stored under -20 ^{o}C for 30 min, and sonicated in an ice bath for 10 min. After centrifuging (14,000 rpm, 10 min), 700 µL supernatant was collected into a new Eppendorf tube. The supernatant was then dried under 37 ^{o}C.

The dried sample was derivatized with 40 µL methoxyamine hydrochloride solution in pyridine (20 mg/mL) under 60 ^{o}C for 90 min. Next, 40 µL N-tert-Butyldimethylsilyl-N-methyltrifluoroacetamide (MTBSTFA) was added and incubated under 60 ^{o}C for 30 min. The sample was then vortexed for 30 s followed by centrifugation at 14,000 rpm for 10 min. Finally, 70 µL supernatant was collected into a new glass vial for gas chromatography mass spectrometry (GC-MS) analysis.

GC-MS analysis was performed using an Agilent 7820A GC-5977B MS system (Agilent Technologies, Santa Clara, CA). Metabolites were separated using an HP-5ms capillary column coated with 5% phenyl-95% methylpolysiloxane (30 m × 250 µm i.d., 0.25 µm film thickness, Agilent J&W Scientific, Folsom, CA). 1 µL of each sample was injected. The solvent delay time was set to 4.5 min. The initial oven temperature was held at 60 ^{o}C for 1 min, ramped to 325 ^{o}C at a rate of 10 ^{o}C/min, and finally held at 325 ^{o}C for 10 min. Helium was used as the carrier gas at a constant flow rate of 20 mL/min through the column. The temperature of the front inlet, transfer line, and electron impact (EI) ion source was set at 250 ^{o}C, 290 ^{o}C, and 230 ^{o}C,

respectively. The EI energy was 70 eV, and the mass spectral data were collected in a full scan mode (m/z 30-600).

Cytokine quantification. Approximately 20 mg of fecal samples from WT C57BL/6J and WT FVB/NJ mice (adolescent and adult ages, males and females, n=5 per group) were mixed with PBS (pH = 7.2 supplemented with 1 mM PMSF [final concentration] and 1X protease inhibitor cocktail [Sigma-Aldrich, catalog number: P8340]) to a final concentration of 100 mg/ml, and were homogenized and centrifuged at 10,000 g at 4 °C for 15 min. The supernatant was collected and diluted 1:1 in the PBS solution described above, and the cytokines were quantified using the Mouse Cytokine Array Pro-inflammatory Focused 10-plex (MDF10) (Eve Technologies Corp., Calgary, Alberta) per manufacturer's instructions. The 10 cytokines that were determined include: granulocyte-macrophage colony-stimulating factor (GM-CSF), interferon gamma (IFNy), interleukin 1 beta (IL-1β), interleukin 2 (IL-2), interleukin 4 (IL-4), interleukin 6 (IL-6), interleukin 10 (IL-10), interleukin 12 (IL-12p70), monocyte chemoattractant protein-1 (MCP-1), and tumor necrosis factor (TNF-α). The ten cytokines were simultaneously quantified in a multiplex panel using a MILLIPLEX Mouse Cytokine/Chemokine 10-plex kit (Millipore, St. Charles, MO, USA) according to the manufacturer's protocol, and was performed using the Luminex™ 100 system (Luminex, Austin, TX, USA). The assay sensitivities of these markers range from 0.4 – 10.9 pg/mL for the 10-plex. Individual analyte values are available in the MILLIPLEX protocol.

***Data analysis*.** Analysis of FASTQ files was conducted using various python scripts in Quantitative Insights Into Microbial Ecology (QIIME) (Caporaso et al., 2010), including de-multiplexing, quality filtering, operational taxonomy unit (OTU) picking, as well as alpha- and beta-diversity determinations. Metagenome functional content was predicted using Phylogenetic Investigation of Communities by Reconstruction of Observed States (PICRUSt) (Langille et al., 2013). Line plots representing the alpha diversity of each group were generated using ggplot2 (v 3.0.0) in R. Three-dimensional Principle Coordinate Analysis (PCoA) plots (beta diversity)

were generated using the weighted UniFrac diversity metric in Emperor (Gigascience). OTUs were visualized using stacked bar plots generated in SigmaPlot (Systat Software, Inc). Hierarchical clustering dendrograms (Ward's minimum variance method, distance scale) of the top significantly abundant taxa (abundance > 0.005% $p < 0.05$) were generated using gplots (v 3.0.1) and RColorBrewer (v 1.1-2) in R. Bar plots representing cytokine concentration, BA concentration, and SCFA concentration were generated using ggplot2 (v 3.0.0) in R. Correlation matrices representing SCFA and taxa associations were generated using reshape2 (v 1.4.3) and ggplot2 (v 3.0.0) in R.

Asterisks (*) represent significant differences between C57BL/6J and FVB/NJ mice, WT and nuclear receptor-gene-null mice ($p < 0.05$), and WT and hPXR-TG mice. Statistically significant differences between WT FVB/NJ and C57BL/6J mice, as well as between WT FVB/NJ and hPXR-TG mice were determined using the student's *t*-test in Microsoft Excel. Statistically significant differences among WT, PXR-null, CAR-null, and PXR-CAR-null mice (all in C57BL/6J background) were determined using one-way ANOVA followed by Duncan's post-hoc test in R using the DescTools package (v 0.99.26), or SPSS (IBM SPSS Statistics).

RESULTS

The overall experimental design is shown in **Figure 1**. Three experimental settings were designed to model the effect of host genetics on gut microbiome. In **Study 1**, two commonly used laboratory mouse strains with known genetic variations(Wong et al., 2012), namely the C57BL/6J and FVB/NJ mice, were selected to determine how general differences in host genetics regulate the composition and function of the gut microbiome. To note, it has been reported that FVB mice had higher hepatic expression of PXR and CAR than C57BL/6J mice(Bradford et al., 2011) (Supplemental Figure 1). In **Study 2**, we focused on the major xenobiotic sensing nuclear receptors PXR and CAR, and examined the necessity of these host

receptors on the basal regulation of gut microbiome, using PXR-null, CAR-null, and PXR-CAR-double null mice (all in C57BL/6J background). In **Study 3**, we compared the gut microbiomes between the mice that carry mPXR vs. the mice that hPXR (both in FVB background), to determine how species-differences of this host drug receptor modulate the gut microbiome.

Study I. Unveiling the effect of host genetics on gut microbiome using two mouse strains (C57BL/6J and FVB/NJ)

Figure 2 shows the alpha diversity (chao1 index), which quantifies the richness of taxa (Figure 2A), as well as the beta diversity, which quantifies the differences in microbiome among different groups (Figure 2B), in male and female C57BL/6J and FVB/NJ mice at adolescent and adult ages. FVB/NJ mice had higher microbial richness compared to their C57BL/6J counterparts in both developmental ages and genders (Figure 2A). Principle coordinates of analysis (PCoA) of the weighted UniFrac measurements showed distinct separations between the microbiomes of FVB/NJ and C57BL/6J mouse strains at both ages and genders (Figure 2B).

Figure 3 shows the compositional changes of the top 15 taxa at the species level as determined by percentage of operational taxonomic units (OTUs). In all groups, the predominant phyla were Bacteroidetes, Firmicutes, Tenericutes, and Verrucomicrobia. Interestingly, *Prevotellaceae Prevotella sp.* had lower relative abundance in FVB/NJ mice as compared to C57BL/6J mice in both ages and genders, while *Paraprevotellaceae Prevotella sp.* was higher in FVB/NJ mice than in C57BL/6J mice at both ages and genders, except for adolescent females. A member of the *Anaeroplasma* genus had higher relative abundance in FVB/NJ mice compared to C57BL/6J mice in all groups except for adult males. Additionally, adolescent male FVB/NJ mice had lower relative abundance of *Ruminococcus gnavus* and a member of the *Oscillospira* genus. The *Turicibacter* genus was higher in both FVB/NJ adolescent males and females as compared to their C57BL/6J counterparts. *A. muciniphila* had higher abundance in adolescent female and adult male FVB/NJ mice than C57BL/6J, with a

tendency in this direction in the other groups as well. The family S24-7 was lower in both FVB/NJ adult gender groups, with a similar trend in the adolescent groups observed. The family Rikenellaceae exhibited higher abundance in adult male FVB/NJ mice than C57BL/6J mice. *Allobaculum sp.* had lower relative abundance in adult female FVB/NJ mice, while bacteria in the genus *Lactobacillus* had higher relative abundance in adult female FVB/NJ mice compared to C57BL/6J mice.

As shown in Supplemental Figure 2, a total of 72 taxa were different between C57BL/6J and FVB/NJ mice. 5 of these taxa, namely *Paraprevotellaceae Prevotella sp.*, *Anaeroplasma sp.*, a member of the RF32 order, *Acinetobacter sp.*, and *Eubacterium dolichum* were higher in relative abundance in FVB/NJ mice in both ages and genders compared to C57BL/6J mice; whereas 4 taxa, namely *Enterococcus sp.*, *Prevotellaceae Prevotella sp.*, *Lactococcus sp.*, and *Carnobacterium sp.* were lower decreased in relative abundance in all groups of FVB/NJ mice compared to C57BL/6J mice.

In summary, profound basal differences in gut microbiome composition were observed between FVB/NJ and C57BL/6J mouse strains.

As shown in Supplemental Figure 3, to predict the metagenomic functional content of the gut microbiome in FVB/NJ and C57BL/6J mice, Phylogenetic Investigation of Communities by Reconstruction of Unobserved States (PICRUSt) was performed (Langille et al., 2013) based on on the QIIME output. Interestingly, between the two mouse strains, males exhibited much more predicted functional changes than females at both ages. Pathways enriched were classified into 5 main groups, namely cellular processes, environmental information processing, genetic information processing, metabolism, and organismal systems. Within cellular processes, 7 were enriched in adolescent male mice, 10 were enriched in adult male mice, and 1 was enriched in adolescent female mice. For environmental information processing, adolescent males had 5 pathways enriched, adult males had 8 pathways enriched, adolescent females had 2 pathways

enriched, and adult females had no enriched pathways. Concerning genetic information processing, adolescent males had 26 pathways enriched, adult males had 29 pathways enriched, 2 pathways were enriched in adolescent females, and no enriched pathways in adult females. Metabolism was the largest category for all groups, with 78 pathways enriched in adolescent males, 104 pathways enriched in adult males, 4 pathways enriched in adolescent females, and 6 enriched in adult females. The last category, organismal systems, had 7 pathways enriched in adolescent males, 5 pathways enriched in adult males, and 1 pathway enriched in each female age group. As shown through the hierarchical clustering dendrograms in Supplemental Figure 3, there was variation between individual mice, but overall, pathways were decreased in C57BL/6J mice and increased in FVB/NJ mice.

As shown in Figure 4, *Lactococcus* was specifically colonized in C57BL/6J mice but not in FVB/NJ mice, and a species in this genus is known to have anti-inflammatory effect (Luerce et al., 2014). Conversely, the pro-inflammatory *Acinetobacter* (Jun et al., 2013; Kikuchi-Ueda et al., 2017), and *E. dolichum*, which is enriched in western diet (Turnbaugh et al., 2009), were specifically colonized in FVB/NJ mice but not in C57BL/6J mice. Therefore, we hypothesized that the basal differences in the gut microbiome of the two mouse strains makes FVB/NJ mice more prone to pro-inflammatory under basal conditions. To assess how strain differences affect inflammation, cytokines were quantified from C57BL/6J and FVB/NJ mice (Figure 5). Overall, pro-inflammatory cytokines were higher in feces of FVB/NJ mice. In particular, MCP-1 had the greatest difference in concentration in all 4 groups, followed by IL-12, and IL-6. TNFα was higher only in FVB/NJ mice only in adult females (Supplemental Figure 4). To note, the anti-inflammatory cytokine IL-10, which is known to increase during inflammation to suppress IL-12 (Rahim et al., 2005), was also higher in FVB/NJ than C57BL/6J mice in males and adult females, indicating a compensatory response.

In summary, these results demonstrate that C57BL/6J and FVB/NJ mice have different gut microbiome compositions that are modified by age and gender. Most notably, the basal differences in gut microbiome may at least partially contribute to higher susceptibility to inflammatory response in FVB/NJ than C57BL/6J mice.

Study II. Understanding the necessity of host nuclear receptors PXR and CAR on the constitutive regulation of the gut microbiome

To determine the necessity of host nuclear receptors on the composition and function of the gut microbiome, 16S rDNA sequencing was conducted on feces collected over a 24-hour period of adolescent and adult aged WT, PXR-null, CAR-null, and PXR-CAR-double null male and female mice (all in C57BL/6J background, n=5 per group). As shown in Figure 6A, regarding alpha diversity PXR and CAR single or double knockout mice tended to have greater richness than WT controls in all groups, and this trend was especially prominent for PXR-CAR double null mice. The only exception was that in adult males, CAR-null mice had the greatest richness as compared to the other genotypes. As shown in Figure 6B, regarding the beta diversity, all 4 genotypes of mice (WT, PXR-null, CAR-null, and PXR-CAR-double null) exhibited distinct separations among their microbial communities at both ages and genders. This indicates that PXR and CAR are important and unique modulators of the gut microbiome.

Figure 7 shows the microbial compositional changes at the species level of the top 15 most abundant bacteria as quantified by percentage of OTUs for the four genotypes of mice (note: the 15th category includes all other taxa summed together). In all exposure groups, the predominant phyla were Bacteroidetes, Firmicutes, and Proteobacteria. The family *S24-7* was lower in all PXR-null and PXR-CAR-double null groups compared to WT feces, as well as in adult CAR-null males. Bacteria in the Clostridiales order were also higher in PXR-null adolescent male and adult female feces, but lower in adolescent male CAR-null and PXR-CAR-null feces. The *Ruminococcaceae* family was also higher in all PXR-null sample groups except

for adolescent females, but this trend is still observed in this group. *Oscillospira sp.* was higher in abundance in adolescent male and adult female PXR-null mice, with this trend seen in the other groups as well. However, the *Oscillospira* genus had lower abundance in PXR-CAR-null samples from adolescent males and females, and in adolescent male CAR-null samples. Bacteria in the family *Helicobacteraceae* increased in relative abundance in PXR-null samples in all groups, as well as both male CAR-null age groups, and CAR-null adult female samples. *Bacteroides sp.* was higher in relative abundance in all PXR-null groups except for adolescent males, and also was higher in all CAR-null groups except for adult males. *Bacteroides sp.* was also higher in both female PXR-CAR-null age groups. A member of the *Rikenellaceae* family was lower in adolescent male CAR-null and both male and adult female PXR-CAR-null samples. A member of the *Lachnospiraceae* family was lower in CAR-null adolescent males but was higher in PXR-null adult males and females. *Sutterella sp.* was higher in CAR-null and PXR-CAR-null in all groups as well as in PXR-null adult males. *Lactobacillus sp.* was higher in all PXR-CAR-null groups. *Allobaculum sp.* was also higher in all PXR-CAR-null groups, except for adult females. *Prevotellaceae Prevotella spp.* was lower in relative abundance in PXR-null adolescent females, adult male CAR-null samples, and adolescent female and both adult PXR-CAR-null sample groups. The species grouped into the other category increased in relative abundance in all PXR-CAR-null samples, as well as CAR-null adolescent females. Individual variations contributing to these differences are displayed in heat map form in Supplemental Figure 5.

In total, 63 taxa with were significantly different between WT and PXR-null, CAR-null, and/or PXR-CAR-null mice (Supplemental Figure 5). Most notably, *Anaerostipes sp.* decreased in relative abundance in all nuclear receptor-deficient mice of both age and genders. A member of the *S24-7* family also decreased in PXR-null and PXR-CAR-null mice of both ages and genders. 13 taxa increased in both ages and genders of at least one nuclear receptor-deficient

genotype of mice, namely *Lactobacillus sp.*, *Adlercreutzia sp.*, *Sutterella sp*., a member of the *Mogibacteriaceae* family, *Desulfovibrio sp*., a member of the *F16* family, a member of the *AF12* family, *Bilophila sp*., *Odoribacter sp*., a member of the *Helicobacteraceae* family, *Bacillus other*, *Paraprevotellaceae Prevotella sp*., and a member of the *Desulfovibrionaceae* family.

To predict how the absence of host nuclear receptors affect the metagenomic functional content of the gut microbiome, PICRUSt was performed, and pathways were categorized using the KEGG system as described in the strain differences section (Supplemental Figure 6). Adolescent and adult females exhibited markedly more functional content predictions than their male counterparts. In both female ages, absence of PXR caused an increase in most pathways, with the converse being true for CAR-null samples. The PXR-CAR-null group appeared to respond to combinatorial effects of absence of PXR or CAR, as no change in the abundance of these pathways was seen for these females. The opposite is true for the samples from male mice in that PXR-CAR-null in both ages, and CAR-null in adult males had a marked increase in pathways compared to PXR-null and WT samples. Therefore, gender and host nuclear receptor status have an effect on the function of the gut microbiome in mice.

As shown in Figure 8, the most notable changes in gut microbiome composition include: 1) the markedly higher abundance of *Lactobacillus sp.* in all PXR-CAR-null groups, and distinct species in the *Lactobacillus* genus are known to carry bile salt hydrolase (BSH) activity to perform BA deconjugation (Ridlon et al., 2016); 2) the markedly lower abundance of *Anaerostipes*, which is known to produce the SCFA butyrate (Kim et al., 2014; Riviere et al., 2016; Baxter et al., 2019), in all 3 knockout mouse strains and especially in the PXR-CAR-double null mice; as well as 3) the apparent higher abundance of *Sutterella,* which is known to be bile-resistant (Williams et al., 2012), in all 3 knockout mouse strains and especially in the CAR-null and PXR-CAR-double null mice. Therefore, we hypothesized that the basal microbial-derived BAs and SCFAs are different among the 4 genotypes of mice.

Figures 9-12 show the BA profiles in WT, PXR-null, CAR-null, and PXR-CAR-double null mice at the two developmental ages and in both genders. In general, major taurine conjugated BAs (T-BAs) were lower (or tended to be lower) in the 3 knockout mouse strains, including a reduction in the primary T-BAs (T-αMCA, T-βMCA, T-CA, and T-CDCA), as well as a reduction in the major secondary BAs (T-ωMCA and THDCA) in feces of adolescent males (Figure 9), a reduction in the primary T-BAs (T-aMCA, T-bMCA, T-CA, and T-CDCA) and the secondary T-BAs (T-ωMCA, T-UDCA, T-HDCA) in feces of adult males (Figure 10), a reduction in the primary BAs (T-αMCA, T-βMCA, T-CA, and T-CDCA) and the secondary T-BAs (T-ωMCA and T-HDCA) in feces of adolescent females (Figure 11), as well as a reduction in the primary T-BAs (T-αMCA and T-βMCA) and the secondary T-BAs (T-ωMCA, T-UDCA, T-HDCA) in feces of adult females (Figure 12). Regarding unconjugated BAs, the secondary BA LCA was higher in adolescent male and female PXR-CAR-double null mice than the corresponding WT controls. In adolescent females, the primary BAs aMCA and bMCA were higher in PXR-null and PXR-CAR-double null mice, and CA was higher in PXR-null mice. The reduction in most T-BAs and increase in certain unconjugated BAs together suggest increased microbial BSH activities in the knockout strains and especially in the PXR-CAR-double null strain. Conversely, in adult males and females, several primary and secondary unconjugated BAs were actually lower in knockout strains than their corresponding WT controls, indicating the presence of other regulatory mechanisms, including a potential reduction in biliary excretion of BAs due to lack of PXR and CAR, because these receptors are known to up-regulate certain bile acid efflux transporters of the host.

Levels of SCFAs and medium chain fatty acids were determined in the 4 genotypes of mice as shown in Supplemental Figure 7. Although the butyrate-producing bacteria *Anaerostipes* was down-regulated in the 3 knockout strains, fecal butyrate levels remained unchanged (data not shown), suggesting the compensatory mechanisms by other bacteria that

are present in these knockout mice. Correlation matrices were generated to illustrate the relationship between bacterial species abundance and SCFA concentration in WT, PXR-null, CAR-null, and PXR-CAR-null mice. Heptanoic acid decreased in CAR-null mice of both female ages as well as adult males, and was negatively correlated with *Sutterella sp.* in these groups as well. Acetic acid increased in relative concentration in adolescent male and adult female groups of nuclear-deficient mice, and also positively correlated with *Sutterella sp., Lactobacillus sp.,* and a member of the *Helicobacteraceae* family in these mice. C 10 was increased in PXR-CAR-null adult male mice, whereas 2-methylbutyric acid increased in PXR-null adolescent male mice.

Study III. Comparison between mouse and human PXR in regulating the gut microbiome

To compare the role of mouse and human PXR genes on the composition and function of the gut microbiome, 16S rDNA sequencing was conducted on feces collected over a 24-hour period of adolescent and adult aged FVB/NJ wild-type (WT) and humanized PXR transgenic (hPXR-TG) male and female mice (n=5 per group). As shown in Figure 13A, adolescent male hPXR-TG mice had greater richness in their fecal microbial community (QIIME, alpha diversity, chao1 index). However, there was no difference in the richness of the gut microbiome in other age or gender groups (data not shown). As shown in Figure 13B, in all 4 comparisons, hPXR-TG and WT mice exhibited distinct separations between their microbial communities as measured by beta diversity (weighted uniFrac).

Figure 13 shows the top 15 species level compositional changes of the gut microbiome as quantified by % OTUs. In all groups, the predominant phyla were Bacteroidetes, Firmicutes, Tenericutes, and Verrucomicrobia, plus Proteobacteria in both adult groups and adolescent males. A member of the Clostridiales order as well as *Anaeroplasma sp.* were lower in abundance in adolescent male and female hPXR-TG samples, while *Sutterella sp.* was higher in both male age groups. *Paraprevotellaceae Prevotella sp.* increased in relative abundance in

adult male and both female age groups hPXR-TG samples whereas *A. muciniphila* was lower in hPXR-TG adult male and both female age groups. The *Lachnospiraceae* family decreased in abundance in adolescent female hPXR-TG mice. A member of the *Ruminococcaceae* family as well as a species in the genus *Ruminococcus* were both lower in adolescent hPXR-TG female samples. Distinctive to adult female hPXR-TG mice, *Bacteroides sp.* increased in relative abundance and *Turicibacter sp.* decreased in abundance. Lastly, the species grouped into other were higher in relative abundance in adolescent hPXR-TG males.

In total, 27 taxa with an abundance above 0.00005 were significantly different between WT and hPXR-TG mice (Supplemental Figure 8). Among those, only a member of the *AF12* genus was higher in hPXR-TG mice of both ages and genders, whereas *Paraprevotellaceae Prevotella sp.* were higher in all groups of hPXR-TG mice except for adolescent males Supplemental Figure 8 and Figure 15). While no taxa consistently decreased in all groups of hPXR-TG mice compared to WT, a member of the RF39 order was lower in all hPXR-TG groups except for adolescent females, and *A. muciniphila* was lower in all hPXR-TG groups except for adolescent males (Supplemental Figure 8 and Figure 15). Overall, it appears that species specificity of PXR (i.e. mPXR vs. hPXR) affects the composition of bacteria in the gut microbiome.

As shown in Supplemental Figure 9, PICRUSt was used to predict the effect of host nuclear receptor genotype on the metagenomic functional content of the gut microbiome in mice. Adult male hPXR-TG mice were the only group with altered functional pathways. These 21 pathways are: lysine degradation, styrene degradation, aminobenzoate degradation, sulfur metabolism, limonene and pinene degradation, atrazine degradation, biosynthesis of siderophore group nonribosomal peptides, biosynthesis of unsaturated fatty acids, arachidonic acid metabolism, retinol metabolism, chlorocyclohexane and chlorobenzene degradation, bacterial invasion of epithelial cells, proximal tubule bicarbonate reclamation, metabolism of

cofactors and vitamins, ion channels, flavonoid biosynthesis, cytochrome P450-mediated xenobiotic metabolism, caprolactam degradation, tryptophan metabolism, and cell motility and secretion. Notably, all of these pathways decreased in the adult male hPXR-TG mice, with some individual variation. Therefore, species specificity of PXR (i.e. mPXR vs. hPXR) affects the predicted functional differences of the gut microbiome, in a gender- and age-specific manner.

As shown in Figure 16, BA profiles were different between WT and hPXR-TG mice. Specifically, the largest increase in relative concentration occurred with the secondary BA DCA in hPXR-TG adult male mice, and this trend was seen in the other groups as well. The primary BA CA, which is the precursor of DCA, also tended to be higher in hPXR-TG mice at all 4 comparisons. Conversely, the major secondary BA T-ωMCA tended to be lower in hPXR-TG mice in all 4 comparisons, whereas its unconjugated form ωMCA also tended to be lower in female hPXR-TG mice. Regarding other minor BAs in feces, HDCA was lower in both hPXR-TG adult mice groups, with this trend observed in the adolescent mice, and UDCA was higher in adolescent male and adult female hPXR-TG mice, with this trend continuing in the other groups as well.

Regarding SCFAs, as shown in Supplemental Figure 10, 2-methylbutyric acid is the only SCFA consistently changed, and so it is decreased in all groups of hPXR-TG mice. 2-methylbutyric acid positively correlates with *A. muciniphila* and negatively correlates *with Paraprevotellaceae Prevotella sp*. in all groups except for adolescent males. Propionic acid increased in both male age groups of hPXR-TG mice, and positively correlated with *Sutterella sp*. Interestingly, butyric acid decreased in relative concentration in adult male hPXR-TG mice compared to WT, positively correlated with *A. muciniphila*, and negatively correlated with *Sutterella sp*. and *Paraprevotellaceae Prevotella sp.*

The weights of the adult mice were recorded as mass in grams (g), as shown in Supplemental Figure 11. Overall, female mice weighed less than male mice. PXR-null, CAR-null, and PXR-CAR-null mice weighed similarly to WT C57BL/6J mice. However, hPXR-TG mice weighed less than WT FVB/NJ mice.

A graphical depiction of some notable results from this study are shown in Figure 17.

DISCUSSION

In conclusion, the present study has determined in 3 independent experimental settings that host genetics, and differences in the xenobiotic-sensing nuclear receptors PXR and CAR in particular, profoundly influence the composition and predicted functions of the gut microbiome, as well as the production of microbial metabolites (using BAs and SCFAs as examples). Specifically, differences in gut microbiome among individuals with genetic variations may at least partially contribute to the basal gut cytokine levels that may predispose certain individuals to GI inflammation. The presence of the drug receptors PXR and CAR prevents the bloom of other types of bacteria that contribute to the richness of the gut microbiome, likely serving a protective mechanism against opportunistic bacteria that may be harmful to the host. The absence of PXR and CAR also leads to an increase in the *Lactobacillus* genus, corresponding to reduced taurine-conjugated BAs. Gender-specific differences were seen in functional predictions between mouse strains as well as between WT and nuclear receptor-deficient mice. Last but not least, species difference in PXR (mPXR vs. hPXR) also profoundly altered the gut microbiome, including higher *Prevotella* as well as lower *A. muciniphila*, both of which are hallmarks of inflammatory bowel disease (Png et al., 2010; Olbjorn et al., 2019), thus cautions need to be paid while using WT mouse models to study PXR and inflammation, as mPXR carriers may be more resistant to GI inflammation than hPXR carriers.

Just as humans have inter-individual and inter-population genetic differences, strains of mice also differ genetically. Multiple studies have explored the effects of a treatment on the gut microbiota of C57BL/6J and FVB/NJ mice, but to date none have examined the basal regulation of the gut microbiome in these mice. The first part of this study creates a model for how host genetic differences affect the composition and function of the gut microbiome using fecal samples as proxy from the two most widely used laboratory strains of mice.

Higher microbial richness (alpha diversity, Chao1 index) was observed in FVB/NJ mice compared to C57BL/6J mice in both ages and genders (Figure 2A), and these strains of mice exhibited distinctly separated communities of microbiota in all groups as well (Figure 2B). The largest difference in relative abundance of bacteria was the lower abundance of *Prevotellaceae Prevotella sp*. in FVB/NJ mice in all groups (Figure 3). The lower levels of *Prevotellaceae Prevotella sp*. in FVB/NJ mice were accompanied by an increase in multiple other taxa, possibly explaining the differing alpha and beta diversities. These taxa were *Paraprevotellaceae Prevotella sp*., *Anaeroplasma sp*., a member of the RF32 order, *Acinetobacter sp*., and *E. dolichum*. Multiple taxa were observed in lower abundance in FVB/NJ mice compared to C57BL/6J mice as well, including *Enterococcus sp.*, *Lactococcus sp*., and *Carnobacterium sp.* (Supplemental Figure 2). The differences in relative abundance of taxa between the strains has also resulted in a gender-specific effect in functional predictions (Supplemental Figure 3). Overall, males of both ages exhibited more functional prediction changes than female mice of both ages, possibly indicating that male mice are more susceptible to the functional changes resulting from differences in taxa between the two strains.

The majority of the species changed between the two strains have been associated with inflammation. For example, *Prevotellaceae Prevotella sp.*, which decreased in relative abundance in FVB/NJ mice, promotes mucosal inflammation by stimulating the Th17 immune response via epithelial cell production of IL-8, IL-6, and CCL20 (Larsen, 2017). *Prevotellaceae*

Prevotella sp. has been further implicated in IBD through its ability to exacerbate DSS-induced colitis via activation of the inflammasome (Elinav et al., 2011). The genus *Enterococcus*, which also decreased in these mice, has been implicated in infection and increasing susceptibility to IBD (Golinska et al., 2013). *Carnobacterium sp*., which is found in both extreme temperature and animal environments, potentially contains mucin-degrading abilities (Iskandar et al., 2017). The genus *Lactococcus* is well known for its anti-inflammatory capabilities, has been shown to ameliorate colitis, and also protects the liver from inflammation (Luerce et al., 2014; Jena et al., 2017). Several taxa were also higher in FVB/NJ mice. *Anaeroplasma sp*., which potentially has anti-inflammatory function by inducing the anti-inflammatory cytokine TGF-β, has also been associated with existing in lower relative abundance in hypercholesterolemia subjects leading to an unfavorable lipid profile (Granado-Serrano et al., 2019). The order RF32 has been correlated with damaged histopathology and colonic inflammation in mice with colitis (Castro-Mejia et al., 2016). *Acinetobacter sp.* has also been correlated with inflammation through the induced signaling of TLR2 and TLR4, which activate the immune response (Erridge et al., 2007). *E. dolichum* has been shown to produce propionate, which potentially contributes to the inflammatory disease relapsing polychondritis (RP) by continuously stimulating intestinal regulatory T (Treg) cells to produce IL-10, leading to hyporesponsiveness of the Treg cells to mitogen stimulation (Shimizu et al., 2018). In addition to this, *E. dolichum* has been associated with Western diets, and frailty (Turnbaugh et al., 2008; Brown et al., 2012; Jackson et al., 2016; Pallister et al., 2017).

Due to the inflammation-related bacterial changes, we decided to measure cytokine levels in these mice (Figure 5). Overall, cytokines increased in relative concentration and abundance in FVB/NJ mice. Interestingly, the largest increase was exhibited by MCP-1, which serves to regulate the migration and infiltration of monocytes, memory T lymphocytes, and natural killer (NK) cells to sites of inflammation, both within mice and humans (Deshmane et al.,

2009). MCP-1 has also been implicated in the clearance of bacteria via increased expression of inducible nitric oxide synthase (Gomes et al., 2013). IL-10, IL-12, and IL-6 increased in relative concentration in FVB/NJ mice as well. The increase in the anti-inflammatory cytokine IL-10 is potentially due to the concomitant increase in IL-12, because it has been shown to be induced during inflammation to suppress IL-12 (Rahim et al., 2005), indicating a compensatory response. Interestingly, the cytokines which increased in FVB/NJ mice are affiliated with a type-1 immune response, with the exception of IL-4, which is implicated in the type-2 immune response in the pathogenesis of asthma (Dunican and Fahy, 2015). The elevation of the type-1 immune response accompanied by the aforementioned bacteria potentially indicates a response to inflammation within the FVB/NJ mice. Whether this type-1 response is caused by LPS from the bacteria or some other mechanism requires further testing. Considering this is an animal study, all variation in experimental parameters was restrained to the strains themselves, potentially indicating a genomic difference-mediated effect. FVB/NJ mice contain the G protein-coupled receptor 84 (GPR84) deletion, which leads to accumulation of triglycerides and kidney fibrosis (Gagnon et al., 2018). In fact, GPR84 mRNA expression is elevated during inflammation, and activation of this receptor led to lowered levels of IL-12, IL-6, and MCP-1 in a study by Gagnon et al, indicating a protective response by this receptor (Gagnon et al., 2018). This effect would explain the phenomenon observed in this study.

These results will inform future research on the gut microbiome using these two mouse models.

In study II, observations on microbial compositional and metabolite changes in nuclear receptor gene null mice have provided new insights into the necessity of these host xenobiotic-sensing nuclear receptors on the regulation of gut microbiome under physiological conditions. Interestingly, the absence of PXR or CAR increased the richness of the gut microbiota, and the absence of both receptors further augmented this increase (Figure 6A). This indicates a

potential bacteriostatic function of PXR and CAR. The absence of these receptors has also resulted in a gender-specific effect in functional predictions (Supplemental Figure 6). Overall, females of both ages exhibited more functional prediction changes than male mice of both ages, possibly indicating that female mice are more susceptible to the functional changes resulting from differences in taxa between WT and nuclear receptor-deficient mice. The absence of these receptors also led to multiple taxa-level differences in abundance. Especially, the markedly higher proportion of the *Lactobacillus* genus in the PXR-CAR-double null mice consistently correspond to a marked decrease in major T-BAs in feces. While *Lactobacillus* is most known for its probiotic potential, many species and strains of the *Lactobacillus* genus have been reported to carry BSH activities that deconjugate the taurine and glycine molecules from BAs (De Smet et al., 1995; Kumar et al., 2006; Ridlon et al., 2006; Chae et al., 2013; Allain et al., 2017; Allain et al., 2018; O'Flaherty et al., 2018; Foley et al., 2019). In mice, the predominant effect is expected to be T-BA deconjugation, because taurine conjugation is a predominant pathway in mice over glycine conjugation. We have previously demonstrated that pharmacological activation of PXR and CAR leads to decreased gene abundance of the BSH in intestinal content (Dempsey et al., 2019). Findings from the present study further support the inhibitory roles of PXR and CAR in the microbial BSH activities.

Lactobacillus tended to be higher in PXR- and/or CAR-single null mice, although a statistical significance was not achieved (Figure 8), whereas the major T-BAs were significantly lower in single receptor gene null mice. This indicates that other bacteria that remain to be characterized may also contribute to T-BA deconjugation in PXR- and CAR-null mice. Conjugated bile acids have been shown to activate the AKT pathway, which leads to glycogen synthesis (Chiang et al., 2013). Therefore, the absence of PXR and/or CAR, which resulted in lower relative levels of conjugated bile acids compared to WT mice, may lead to impaired glucose homeostasis, possibly increasing the risk for metabolic disease.

Interestingly, although most abundant T-BAs were lower in the PXR-null, CAR-null, and PXR-CAR-double null mice, the unconjugated BAs did not increase in feces, except for the adolescent females, where there was an apparent increase in unconjugated αMCA, βMCA in all 3 null mouse genotypes, as well as an increase in CA in PXR-null mice, and these 3 unconjugated BAs are all major primary BAs synthesized from liver. Conversely, certain unconjugated secondary BAs were lower in the receptor gene-null mice, and this pattern was especially prominent in the adult age for all the 3 null genotypes. This indicates that the absence of the host PXR and/or CAR receptor may negatively impact the microbial dehydroxylase activities, either through lowering the bacteria that carry the dehydroxylase genes, or through inhibiting the enzyme activities, through altering the intestinal environment through mechanisms that remain to be characterized.

The last part of this study examined the species differences of PXR on the gut microbiome, by comparing humanized-PXR-transgenic (hPXR-TG) mice and WT mice with murine PXR, both within the FVB/NJ background. Even though murine PXR and human PXR share roughly 82% DNA and 77% protein identity, differences in gut microbiome composition were observed between the two mouse genotypes (NCBI HomoloGene).

While higher microbial richness (alpha diversity, Chao1 index) was only observed in adolescent male hPXR-TG mice compared to WT, fecal microbial communities were strikingly separated (beta diversity) between the PXR species types in both ages and genders (Figure 13B). While *Paraprevotellaceae Prevotella sp*. was responsible for the largest increase in relative abundance in hPXR-TG mice compared to WT, multiple other taxa increased as well, including *AF12 sp*. (Figure 14 & Supplemental Figure 8). Interestingly, a member of the *Christensenellaceae* family and *Desulfovibrio sp*. increased in relative abundance only in adolescent hPXR-TG mice of both genders, and *Parabacteroides sp*., a member of the Bacteroidales order, and a member of the YS2 order increased only in adult hPXR-TG mice of

both genders, possibly showing an age-mediated species effect of PXR on gut microbiota. Taxa decreased in hPXR-TG mice as well, most notably including a member of the RF39 order (class Mollicutes) and *A. muciniphila*. An age effect persisted as well in that a member of the Clostridiales order and *Anaeroplasma sp*. decreased solely in adolescent hPXR-TG mice (Supplemental Figure 8).

The large increase in *Paraprevotellaceae Prevotella sp*. in hPXR-TG mice may partially explain the differences in beta diversity observed between the two PXR species differences. Bacteria in this family have been associated with traditional societies' microbiota, with multiple studies finding a correlation between *Paraprevotellaceae* abundance and carbohydrate-heavy diets (Wu et al., 2011; Acharya et al., 2017; Li et al., 2017b). Interestingly, male hPXR-TG mice of both ages exhibited an increase in relative concentration of propionic acid compared to WT mice, which is a conjugate form of the SCFA propionate (Supplemental Figure 10). A study by Yun et al. found that *Paraprevotellaceae* contributes to propionate formation in a Korean cohort, and this effect is mirrored in another study by Li et al, where an increase in *Paraprevotellaceae* is correlated with increase in propionate, acetate, and butyrate in silk deer fed oak leaves (Li et al., 2015; Yun et al., 2017). Therefore, the observed increase in propionate in male hPXR-TG mice raises the possibility that this is related to the increased relative abundance of *Paraprevotellacea Prevotella sp*.

A member of the *AF12* genus also increased in relative abundance in all groups of hPXR-TG mice. *AF12 sp*. is an under-characterized microbe, with some literature finding a correlation between higher abundance and lower body weight, although some evidence is conflicting (Garcia-Mazcorro et al., 2016; Alteber et al., 2018; Chen et al., 2018; Lai et al., 2018). Interestingly, hPXR-TG mice were lower in body weight compared to their WT equivalents in our study (Supplemental Figure 11). Additionally, *AF12 sp*. has been observed to increase in relative abundance after dietary supplementation of the herbal remedies

daikenchuto and the Lingzhi mushroom (*G. lucidum*) (Meneses et al., 2016; Miyoshi et al., 2018). In particular, in Meneses et al, the increase in relative abundance of *AF12* after Lingzhi mushroom consumption by C57BL/6J mice was followed by lowered cholesterol and greater excretion of fecal bile acids (Meneses et al., 2016). This study observed increased levels of cholic acid (CA) and deoxycholic acid (DCA) in hPXR-TG mice, which may be related to the increase in *AF12 sp*. (Figure 16).

Lastly, *A. muciniphila* decreased in relative abundance in hPXR-TG mice. *A muciniphila* is a notable bacterial species with mucin-degrading abilities, which has been linked to anti-inflammatory function in liver injury and in diseases such as inflammatory bowel disease (IBD), potentially through its ability to improve an injured gut barrier (Reunanen et al., 2015; Wu et al., 2017; Zhao et al., 2017; Ring et al., 2019). Therefore, this decrease in *A. muciniphila* may lead to a susceptibility for hPXR-TG mice to IBD. Interestingly, hPXR-TG mice are used to study IBD, such as in Dou et al, where hPXR-TG mice were treated with DSS to induce colitis, and then treated with isorhamnetin, a PXR agonist in order to study its effects on ameliorating IBD (Dou et al., 2014). The propensity for hPXR-TG mice to already be predisposed to colitis through decreased *A. muciniphila* before DSS treatment throws into question the mechanisms by which PXR agonist IBD treatments work – do they treat the underlying *A. muciniphila* underabundance or the damage caused by DSS; or both? In another study, Cheng et al treated hPXR-TG mice with rifaximin, a potent PXR agonist used to treat IBD, and found that chronic exposure to rifaximin causes hepatic steatosis, compared to treated WT and treated PXR-null mice (Cheng et al., 2012). As noted above, hPXR-TG mice are deficient in *A. muciniphila*, potentially increasing their susceptibility to inflammation and liver injury, and so the results in this study may be due to the presence of hPXR rather than rifaximin.

DCA is a bacterially derived secondary bile acid which has been shown to correlate with colon cancer (Ajouz et al., 2014). DCA increased in hPXR-TG mice, possibly indicating that

human PXR increases susceptibility to colon cancer compared to its mouse equivalent. Interestingly, CA was also increased in hPXR-TG mice, possibly indicating that DCA was formed via bacterial deconjugation mechanisms. This proposed mechanism is further confirmed by the observation that the conjugated form of CA, taurocholic acid (TCA), was unchanged, indicating CA and DCA were not increased through *de novo* synthesis in the liver.

This is the first study to characterize the gender- and age-related differences between human and murine PXR on the gut microbiome, which should be considered in future research using mice to predict inflammation- and bile acid-related outcomes in humans.

FOOTNOTE

Supported by National Institutes of Health (NIH) grant ES025708, ES030197, GM111381, the University of Washington Center for Exposures, Diseases, Genomics, and Environment [P30 ES0007033], and the Murphy Endowment.

Figure 1

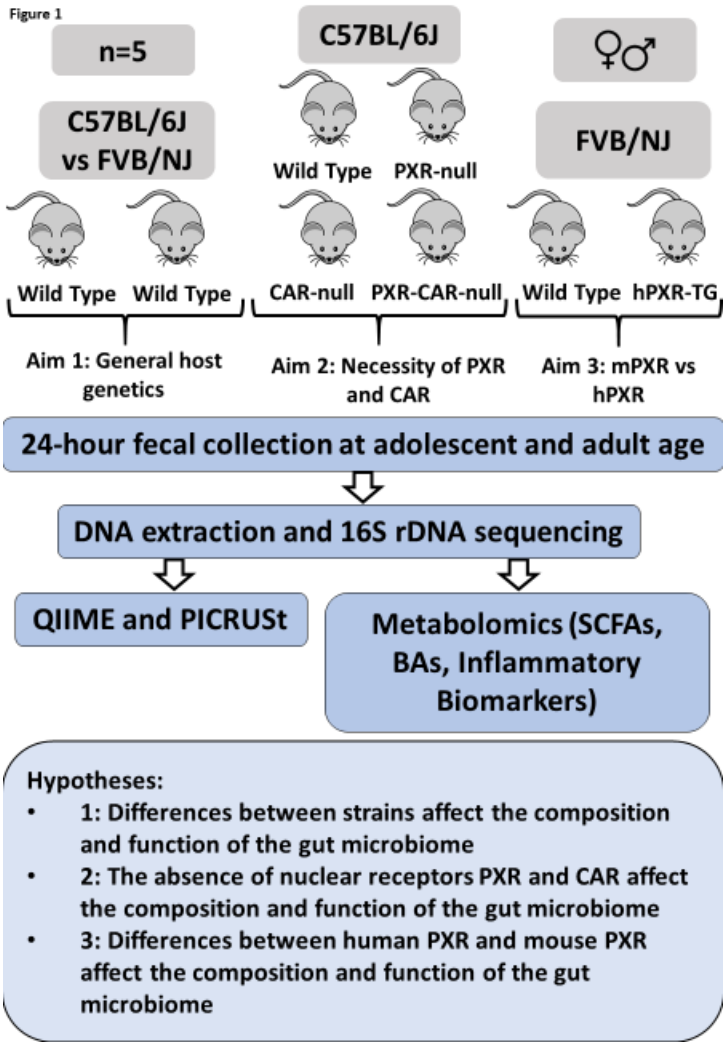

Hypotheses:

- 1: Differences between strains affect the composition and function of the gut microbiome
- 2: The absence of nuclear receptors PXR and CAR affect the composition and function of the gut microbiome
- 3: Differences between human PXR and mouse PXR affect the composition and function of the gut microbiome

Figure 2

$p < 0.05$, *t*-test

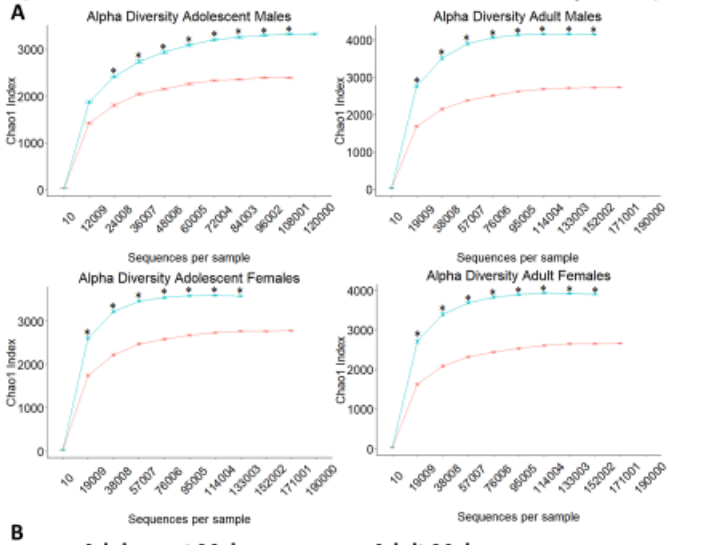

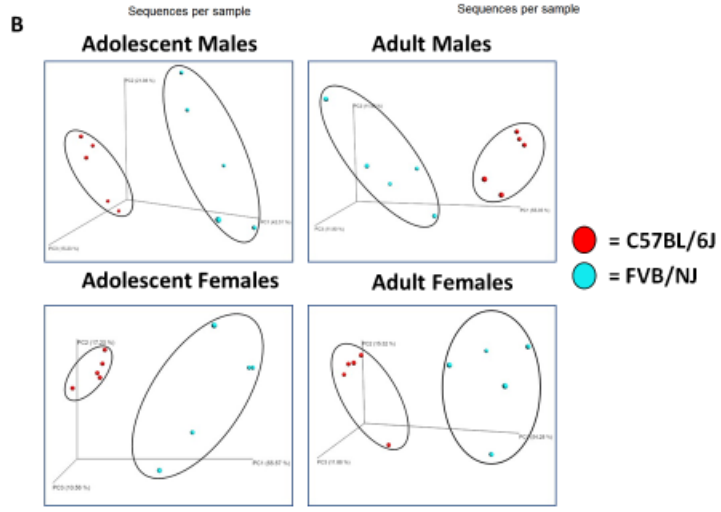

Figure 3

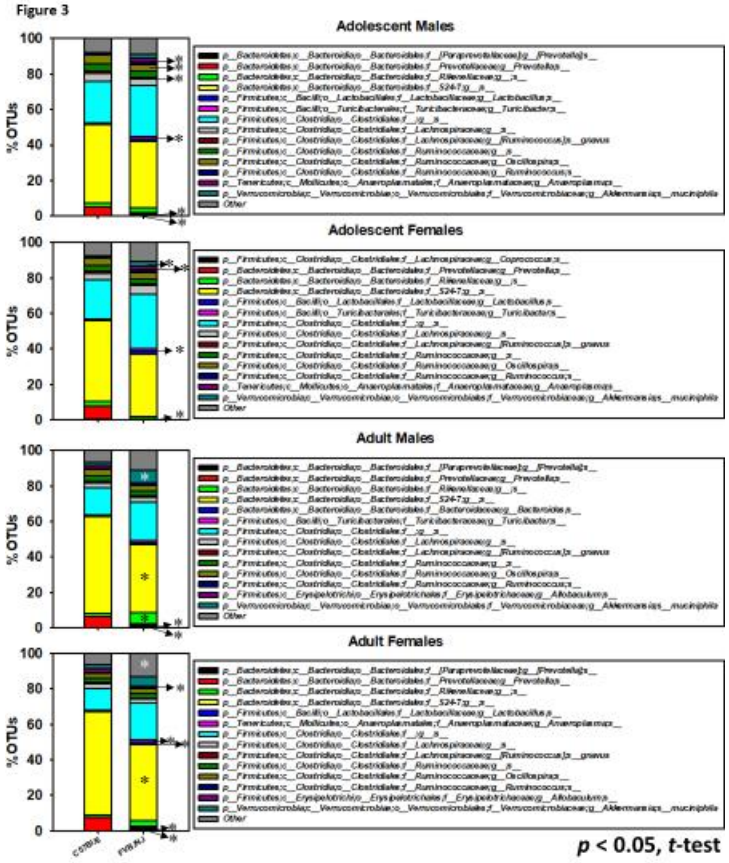

$p < 0.05$, *t*-test

Figure 4

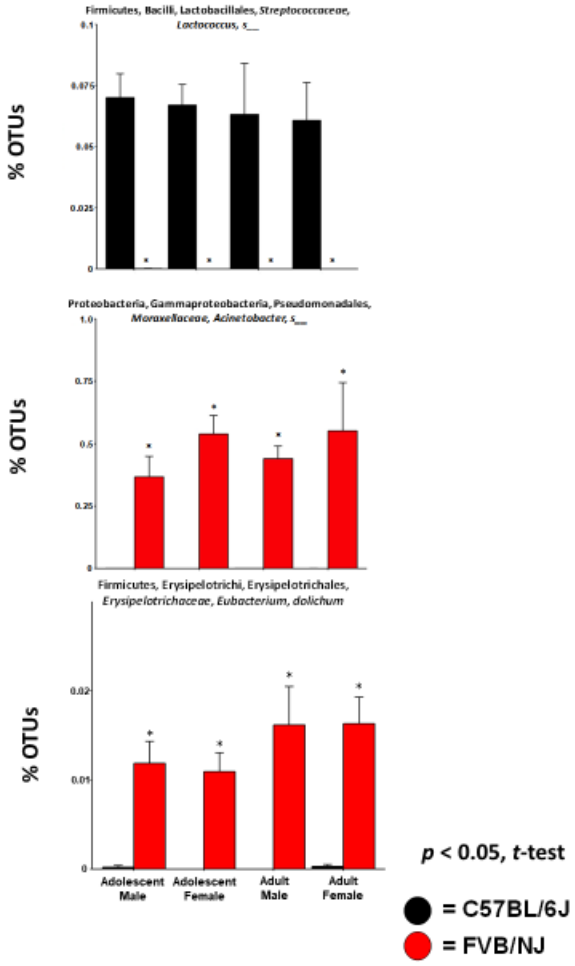
Firmicutes, Bacilli, Lactobacillales, Streptococcaceae, Lactococcus, s__
% OTUs
Proteobacteria, Gammaproteobacteria, Pseudomonadales, Moraxellaceae, Acinetobacter, s__
% OTUs
Firmicutes, Erysipelotrichi, Erysipelotrichales, Erysipelotrichaceae, Eubacterium, dolichum
% OTUs
Adolescent Male
Adolescent Female
Adult Male
Adult Female
p < 0.05, t-test
= C57BL/6J
= FVB/NJ

Figure 5

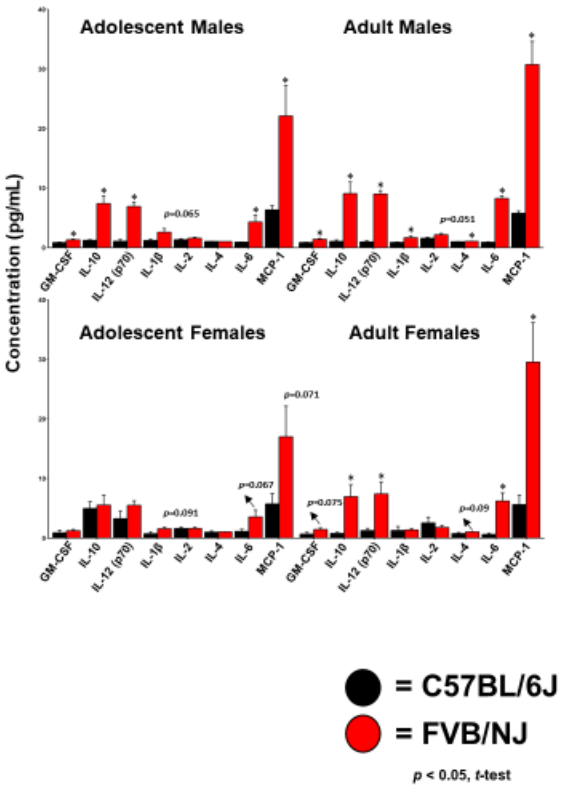
Adolescent Males
Adult Males
Adolescent Females
Adult Females
Concentration (pg/mL)
GM-CSF
IL-10
IL-12 (p70)
IL-1β
IL-2
IL-4
IL-6
MCP-1
p=0.065
p=0.051
p=0.071
p=0.067
p=0.075
p=0.091
p=0.09
= C57BL/6J
= FVB/NJ
p < 0.05, t-test

Figure 6

$p < 0.05$, ANOVA with Duncan's test

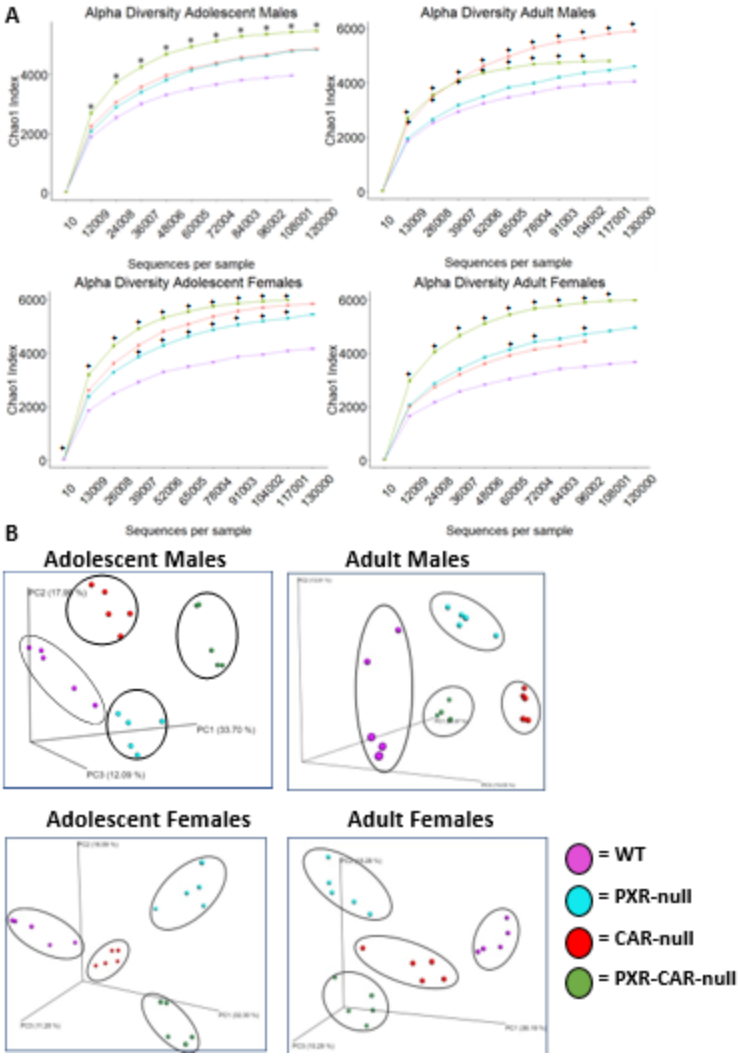

Figure 7

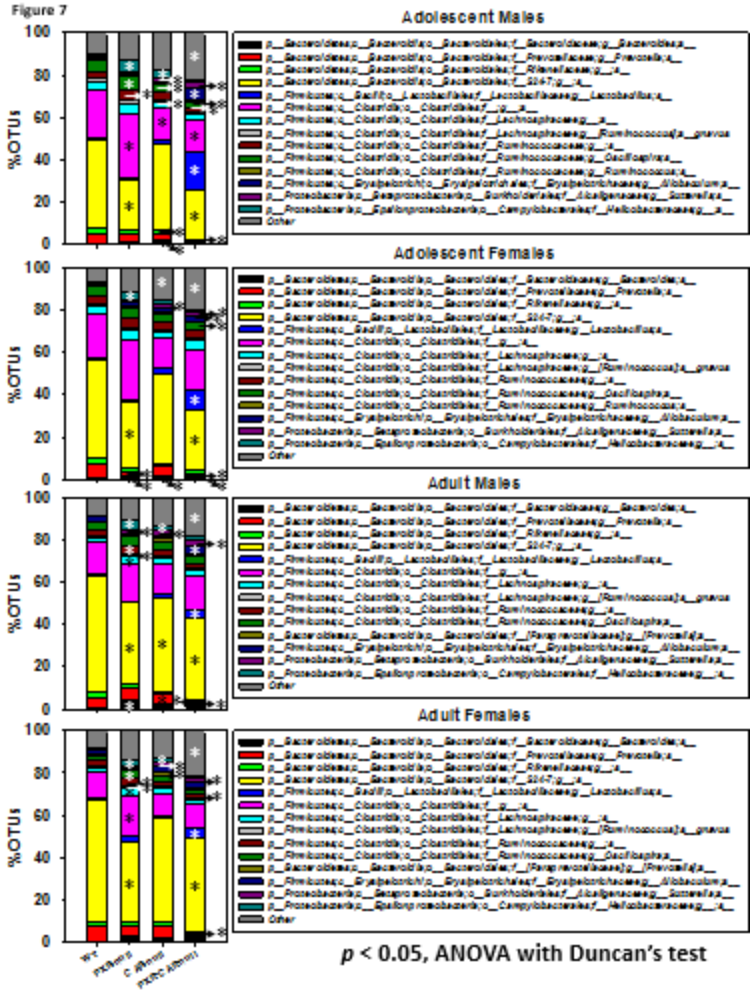

$p < 0.05$, ANOVA with Duncan's test

Figure 8

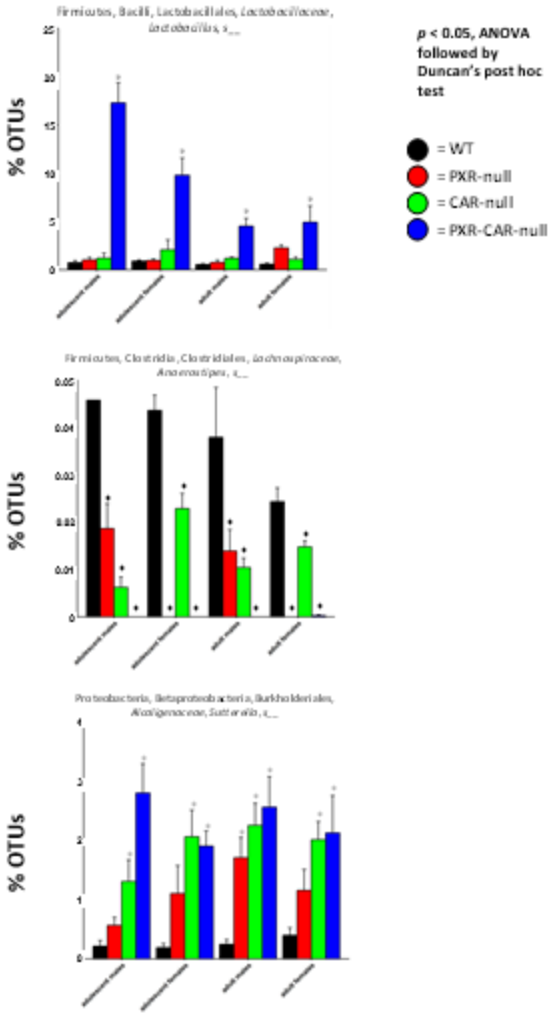

$p < 0.05$, ANOVA followed by Duncan's post hoc test

= WT
= PXR-null
= CAR-null
= PXR-CAR-null

Figure 9

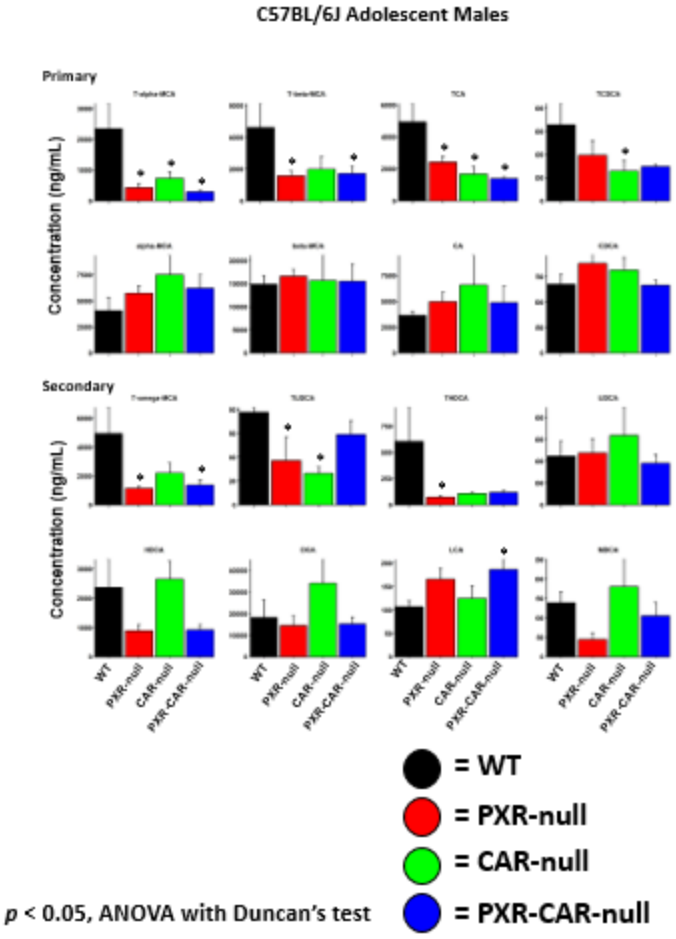

$p < 0.05$, ANOVA with Duncan's test

Figure 10

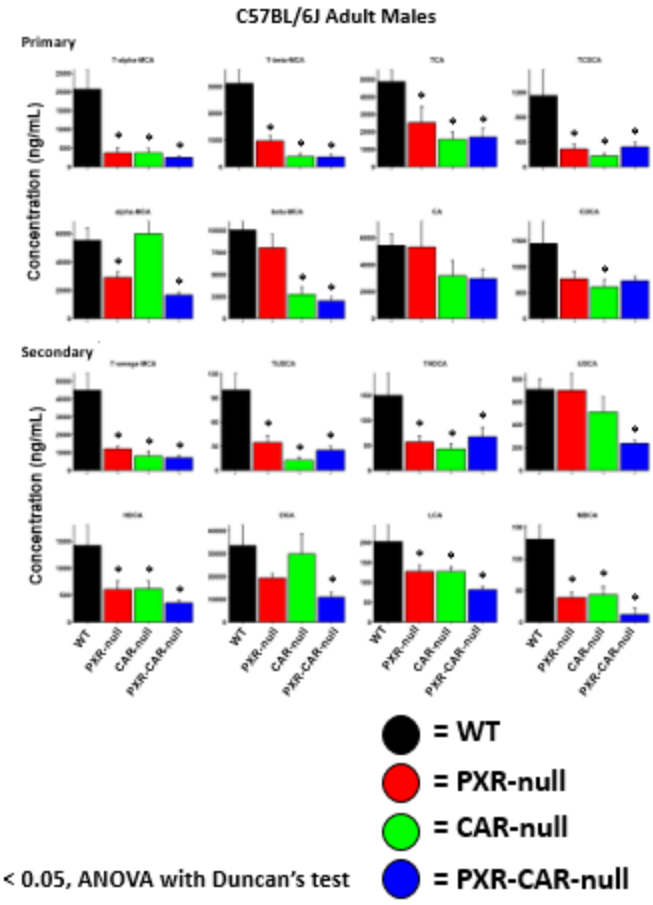

$p < 0.05$, ANOVA with Duncan's test

Figure 11

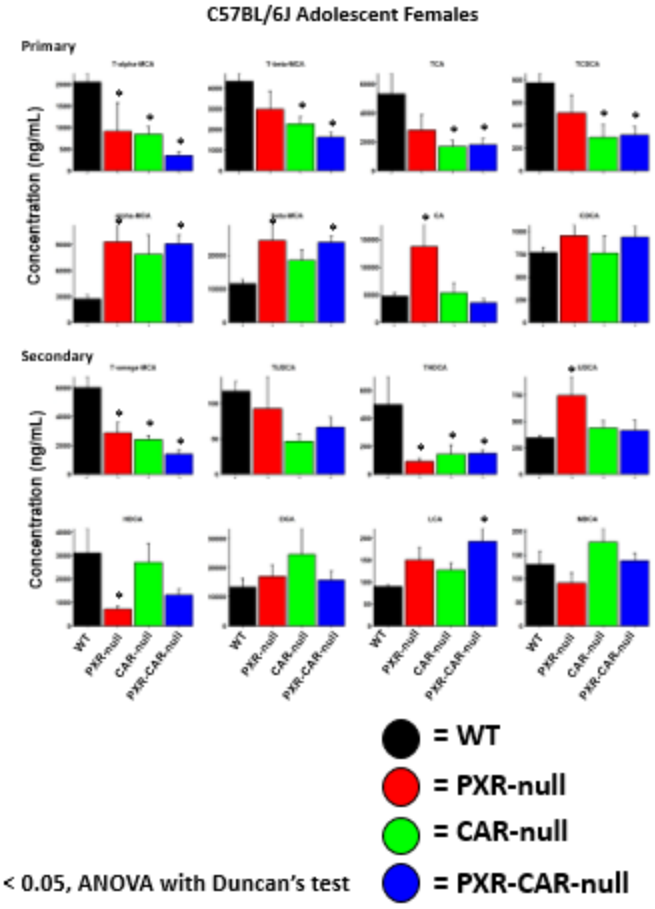

$p < 0.05$, ANOVA with Duncan's test

Figure 12

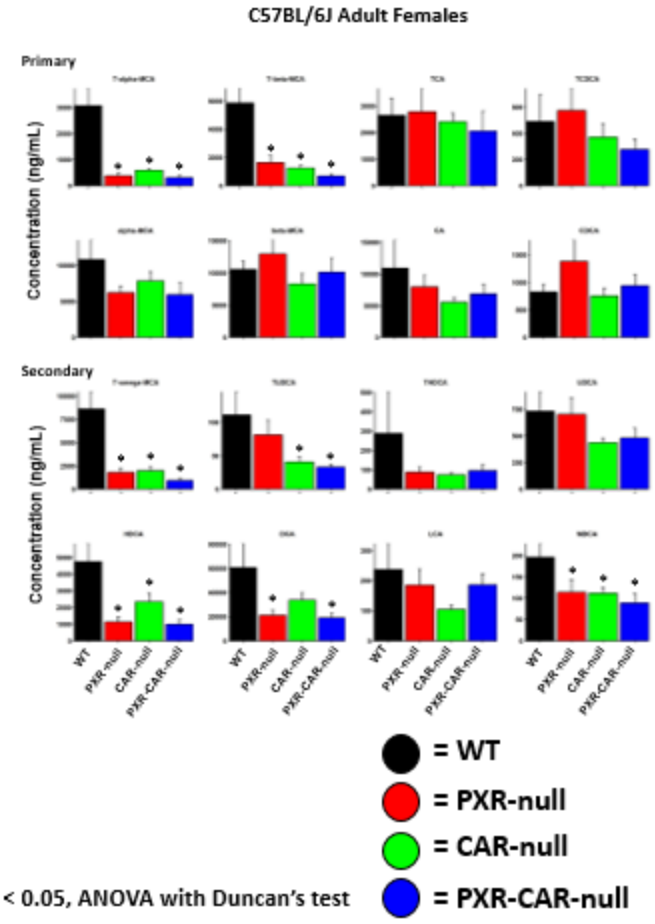

$p < 0.05$, ANOVA with Duncan's test

Figure 13

$p < 0.05$, *t*-test

A

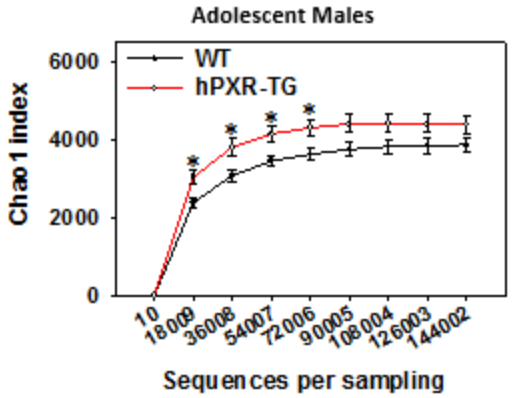

B

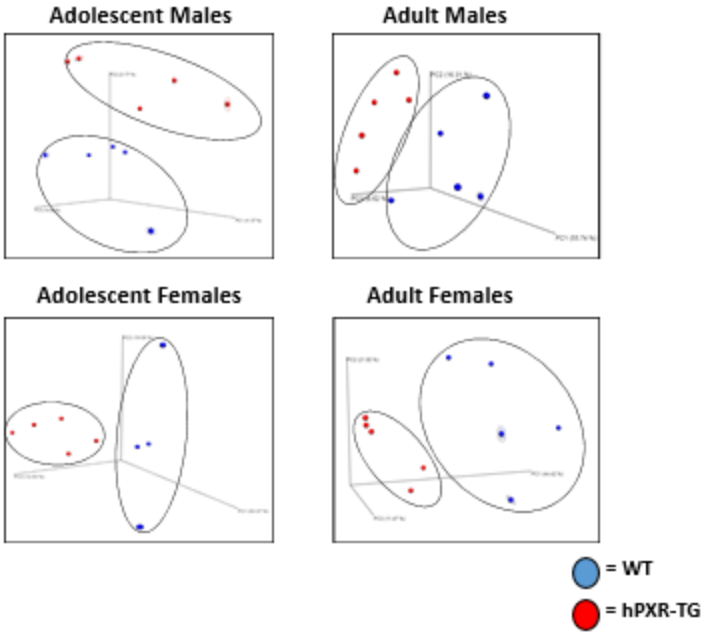

Figure 14

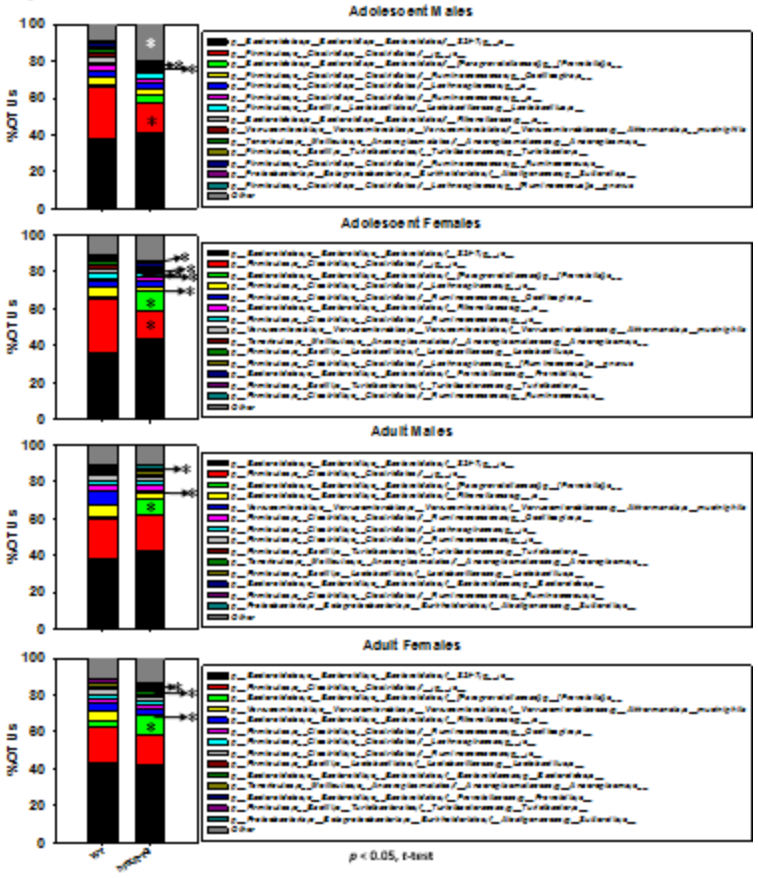
Adolescent Males
Adolescent Females
Adult Males
Adult Females
%OTUs
0
20
40
60
80
100
WT
SYNGAP
Other
p < 0.05, t-test

Figure 15

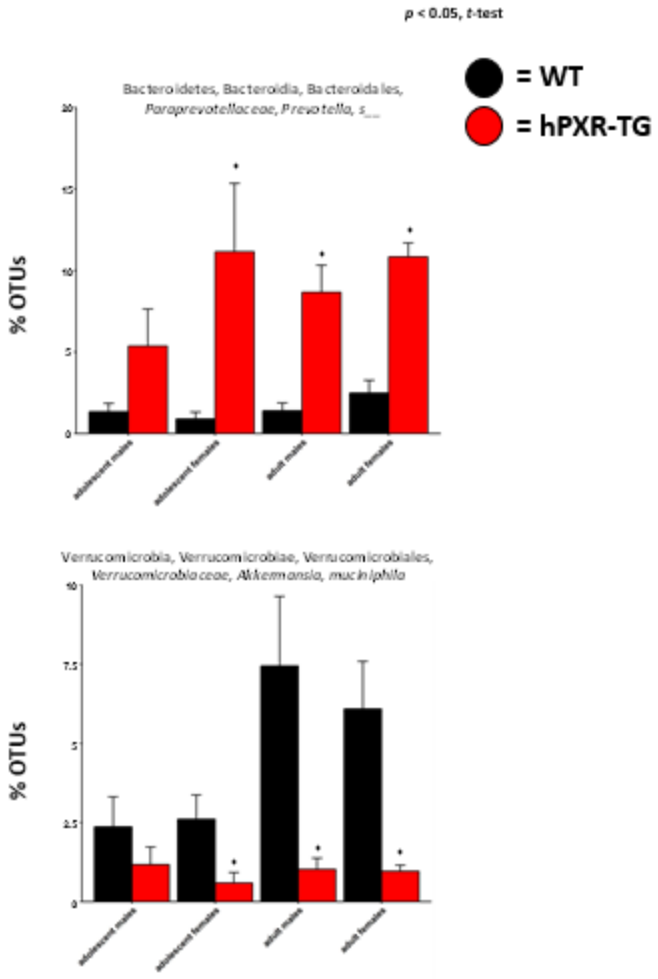
p < 0.05, t-test
= WT
= hPXR-TG
Bacteroidetes, Bacteroidia, Bacteroidales, Paraprevotellaceae, Prevotella, s__
% OTUs
adolescent males
adolescent females
adult males
adult females
Verrucomicrobia, Verrucomicrobiae, Verrucomicrobiales, Verrucomicrobiaceae, Akkermansia, muciniphila
% OTUs
adolescent males
adolescent females
adult males
adult females

Figure 16

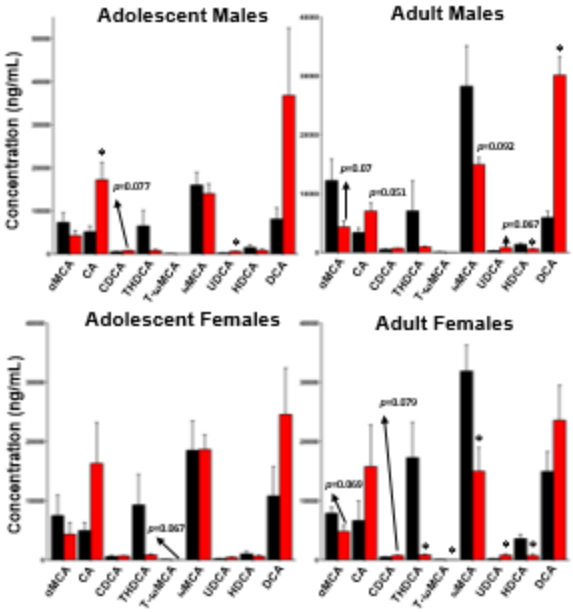

$p < 0.05$, *t*-test

● = WT

● = hPXR-TG

Figure 17

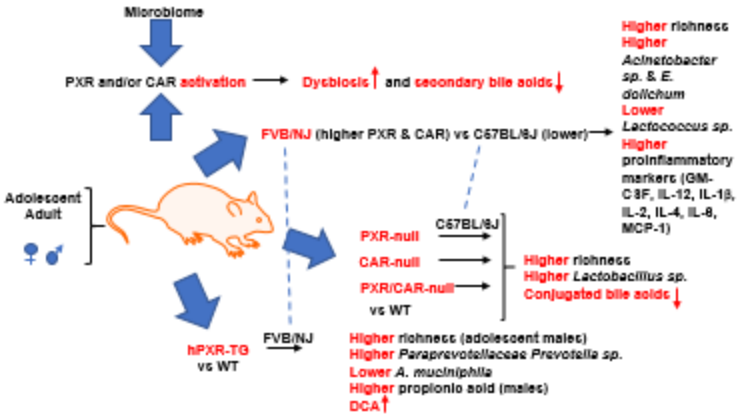

Supplemental Table 1: Optimized UPLC/MS-MS gradient for bile acid chromatography

Time (minute)	Mobile phase A (%) (10mM ammonium acetate with 20% Acetonitrile in water)	Mobile phase B (%) (10 mM ammonium acetate with 80% Acetonitrile in water)
0.00	95	5
5.00	95	5
14.00	86	14
14.50	75	25
17.50	75	25

18.00	50	50
22.00	50	50
22.50	20	80
24.50	20	80
25.00	95	5

FIGURE LEGENDS

Figure 1. A diagram of the experimental design of the study. To compare the role of strain differences on the composition and function of the gut microbiome, fecal samples were collected from WT C57BL/6J and WT FVB/NJ male and female mice of adolescent and adult ages (n=5 of each group). To determine the necessity of host nuclear receptors on the composition and function of the gut microbiome, fecal samples were collected from WT, PXR-null, CAR-null, and PXR-CAR-null male and female mice of adolescent and adult ages (n=5 of each group). To compare the role of mouse and human PXR genes on the composition and function of the gut microbiome, fecal samples were collected from WT and hPXR-TG FVB/NJ male and female mice of adolescent and adult ages (n=5 of each group). Fecal samples were collected after 24 hours and 16S rDNA sequencing was conducted by amplifying the hypervariable V4 region. Analysis of FASTQ files was conducted using various python scripts in Quantitative Insights Into Microbial Ecology (QIIME)(Caporaso et al., 2010), including de-multiplexing, quality filtering, operational taxonomy unit (OTU) picking, as well as alpha- and beta-diversity determinations. Metagenome functional content was predicted using Phylogenetic Investigation of Communities by Reconstruction of Observed States (PICRUSt) (Langille et al., 2013). BAs were quantified using liquid chromatography–tandem mass spectrometry (LC-MS/MS). SCFAs were quantified using GC-MS analysis which was performed using an Agilent 7820A GC-5977B MS system (Agilent Technologies, Santa Clara, CA). Cytokines were quantified using the Mouse Cytokine Array Pro-inflammatory Focused 10-plex (MDF10) (Eve Technologies Corp., Calgary, Alberta).

Figure 2. Alpha and beta diversities of C57BL/6J and FVB/NJ mice. A. Alpha diversity of gut microbiota within C57BL/6J and FVB/NJ mice. Line plots were generated using the R package ggplot. Asterisks represent statistically significant differences compared to C57BL/6J mice (*t*-test, $p < 0.05$). **B.** Principal components analysis (PCA) plots showing the beta diversities of adolescent male, adult male, adolescent female, and adult female C57BL/6J and FVB/NJ mice.

Figure 3. Proportional OTUs in C57BL/6J and FVB/NJ mice. Stacked bar chart illustrating the percentage of differentially regulated taxa in fecal samples in C57BL/6J and FVB/NJ male and female, adolescent and adult mice. The top 14 differentially abundant taxa in each group were plotted and all other detected taxa were summed together to form the Other category. Asterisks represent statistically significant differences compared to C57BL/6J mice (*t*-test, $p < 0.05$).

Figure 4. Percentage OTUs of *Lactococcus sp*., *Acinetobacter sp*., and *E. dolichum*. Individual barplots of *Lactococcus sp*., *Acinetobacter sp*., and *E. dolichum*, as generated by the R package ggplot2. Asterisks represent statistically significant differences compared to C57BL/6J mice (*t*-test, $p < 0.05$).

Figure 5. Cytokine concentrations in C57BL/6J and FVB/NJ mice. Side by side bar plots of cytokine concentrations (pg/mL) as generated by the R package ggplot2. Asterisks represent statistically significant differences compared to C57BL/6J mice (*t*-test, $p < 0.05$).

Figure 6. Alpha and beta diversities of C57BL/6J WT, PXR-null, CAR-null, and PXR-CAR-null mice. A. Alpha diversity of gut microbiota within C57BL/6J WT, PXR-null, CAR-null, and PXR-CAR-null mice. Line plots were generated using the R package ggplot. Asterisks represent statistically significant differences compared to WT mice (one-way ANOVA, Duncan's post hoc, $p < 0.05$). **B.** Principal components analysis (PCA) plots showing the beta diversities of adolescent male, adult male, adolescent female, and adult female C57BL/6J WT, PXR-null, CAR-null, and PXR-CAR-null mice.

Figure 7. Proportional OTUs of C57BL/6J WT, PXR-null, CAR-null, and PXR-CAR-null mice. Stacked bar chart illustrating the percentage of differentially regulated taxa in fecal samples in C57BL/6J WT, PXR-null, CAR-null, and PXR-CAR-null male and female, adolescent and adult mice. The top 14 differentially abundant taxa in each group were plotted and all other

detected taxa were summed together to form the Other category. Asterisks represent statistically significant differences compared to WT mice (one-way ANOVA, Duncan's post hoc, $p < 0.05$).

Figure 8. Percentage OTUs of *Lactobacillus sp*., *Anaerostipes sp*., and *Sutterella sp*. Individual barplots of *Lactobacillus sp*., *Anaerostipes sp*., and *Sutterella sp.*, as generated by the R package ggplot2. Asterisks represent statistically significant differences compared to WT mice (one-way ANOVA, Duncan's post hoc, $p < 0.05$).

Figure 9. BA concentrations in C57BL/6J WT, PXR-null, CAR-null, and PXR-CAR-null adolescent male mice. Individual bar plots of BA concentrations (ng/mL) in adolescent male, mice as generated by the R package ggplot2. BAs were quantified by LC MS/MS as described in MATERIALS AND METHODS. Asterisks represent statistically significant differences compared to WT mice (one-way ANOVA, Duncan's post hoc, $p < 0.05$).

Figure 10. BA concentrations in C57BL/6J WT, PXR-null, CAR-null, and PXR-CAR-null adult male mice. Individual bar plots of BA concentrations (ng/mL) in adult male, mice as generated by the R package ggplot2. BAs were quantified by LC MS/MS as described in MATERIALS AND METHODS. Asterisks represent statistically significant differences compared to WT mice (one-way ANOVA, Duncan's post hoc, $p < 0.05$).

Figure 11. BA concentrations in C57BL/6J WT, PXR-null, CAR-null, and PXR-CAR-null adolescent female mice. Individual bar plots of BA concentrations (ng/mL) in adolescent female, mice as generated by the R package ggplot2. BAs were quantified by LC MS/MS as described in MATERIALS AND METHODS. Asterisks represent statistically significant differences compared to WT mice (one-way ANOVA, Duncan's post hoc, $p < 0.05$).

Figure 12. BA concentrations in C57BL/6J WT, PXR-null, CAR-null, and PXR-CAR-null adult female mice. Individual bar plots of BA concentrations (ng/mL) in adult female, mice as

generated by the R package ggplot2. BAs were quantified by LC MS/MS as described in MATERIALS AND METHODS. Asterisks represent statistically significant differences compared to WT mice (one-way ANOVA, Duncan's post hoc, $p < 0.05$).

Figure 13. Alpha and beta diversities of WT and hPXR-TG mice. A. Alpha diversity of gut microbiota within WT and hPXR-TG FVB/NJ adolescent male mice. Line plots were generated using SigmaPlot. Asterisks represent statistically significant differences compared to WT mice (*t*-test, $p < 0.05$). **B.** Principal components analysis (PCA) plots showing the beta diversities of adolescent male, adult male, adolescent female, and adult female WT and hPXR-TG mice.

Figure 14. Proportional OTUs of WT and hPXR-TG FVB/NJ mice. Stacked bar chart illustrating the percentage of differentially regulated taxa in fecal samples in WT and hPXR-TG FVB/NJ male and female, adolescent and adult mice. The top 14 differentially abundant taxa in each group were plotted and all other detected taxa were summed together to form the Other category. Asterisks represent statistically significant differences compared to WT mice (*t*-test, $p < 0.05$).

Figure 15. Percentage OTUs of *Paraprevotellaceae Prevotella sp*. and *A. muciniphila*. Individual barplots of *Paraprevotellaceae Prevotella sp*. and *A. muciniphila*, as generated by the R package ggplot2. Asterisks represent statistically significant differences compared to WT mice (*t*-test, $p < 0.05$).

Figure 16. BA concentrations in WT and hPXR-TG FVB/NJ mice. Side by side bar plots of BA concentrations (ng/mL) in WT and hPXR-TG mice as generated by the R package ggplot2. BAs were quantified by LC MS/MS as described in MATERIALS AND METHODS. Asterisks represent statistically significant differences compared to WT mice (*t*-test, $p < 0.05$).

Figure 17. Summary of conclusions. A graphical depiction of the conclusions reached in this study.

Supplemental Figure 1. Expression values of PXR and CAR in livers of C57BL/6J and FVB/NJ mice.

Bar plots of expression values of PXR and CAR in livers of C57BL/6J and FVB/NJ mice from the published data set by Bradford et al., 2011. Bar plots were generated using Geo Profiles of PubMed.

Supplemental Figure 2. Differentially abundant taxa in C57BL/6J and FVB/NJ mice.

Two-way hierarchical clustering of the differentially abundant taxa in fecal samples from adolescent- and adult-aged male and female C57BL/6J and FVB/NJ mice, as generated by the R packages gplots and RColorBrewer. Asterisks represent statistically significant differences compared to C57BL/6J mice (*t*-test, $p < 0.05$).

Supplemental Figure 3. Functional predictions in C57BL/6J and FVB/NJ mice.

Two-way hierarchical clustering dendrograms of differentially regulated KEGG pathways predicted by PICRUSt, as described in *Materials and Methods,* from adolescent- and adult-aged male and female C57BL/6J and FVB/NJ mice (*t*-test, $p < 0.05$). Generated by the R packages gplots and RColorBrewer.

Supplemental Figure 4. IFNγ and TNFα concentrations in C57BL/6J and FVB/NJ mice.

Individual bar plots of IFNγ concentrations (pg/mL) in adolescent and adult, male and female C57BL/6J and FVB/NJ mice and TNFα concentrations (pg/mL) in adult female C57BL/6J and FVB/NJ mice as generated by the R package ggplot2. Asterisks represent statistically significant differences compared to C57BL/6J mice (*t*-test, $p < 0.05$).

Supplemental Figure 5. Differentially abundant taxa in C57BL/6J WT, PXR-null, CAR-null, and PXR-CAR-null mice.

Two-way hierarchical clustering of the differentially abundant taxa in fecal samples from adolescent- and adult-aged male and female C57BL/6J WT, PXR-null, CAR-null, and PXR-CAR-null mice, as generated by the R packages gplots and RColorBrewer. Asterisks represent statistically significant differences compared to WT mice (*one-way ANOVA*, Duncan's post hoc, $p < 0.05$).

Supplemental Figure 6. Functional predictions in C57BL/6J WT, PXR-null, CAR-null, PXR-CAR-null mice.

Two-way hierarchical clustering dendrograms of differentially regulated KEGG pathways predicted by PICRUSt, as described in *Materials and Methods,* from adolescent- and adult-aged male and female C57BL/6J WT, PXR-null, CAR-null, PXR-CAR-null mice (*one-way ANOVA*, Duncan's post hoc, $p < 0.05$). Generated by the R packages gplots and RColorBrewer.

Supplemental Figure 7. SCFA concentrations in C57BL/6J WT, PXR-null, CAR-null, and PXR-CAR-null mice.

Correlation plots of SCFA concentrations and differentially abundant bacteria chosen from the top 15 taxa as generated by the R packages ggplot2 and corrplot. Individual plots of significantly changed SCFAs in C57BL/6J WT, PXR-null, CAR-null, and PXR-CAR-null mice. Asterisks represent statistically significant differences compared to WT mice (*one-way ANOVA*, Duncan's post hoc, $p < 0.05$).

Supplemental Figure 8. Differentially abundant taxa in WT and hPXR-TG FVB/NJ mice.

Two-way hierarchical clustering of the differentially abundant taxa in fecal samples from adolescent- and adult-aged male and female WT and hPXR-TG FVB/NJ mice, as generated by the R packages gplots and RColorBrewer. Asterisks represent statistically significant differences compared to WT mice (*t-test*, $p < 0.05$).

Supplemental Figure 9. Functional predictions in WT and hPXR-TG FVB/NJ mice.

Two-way hierarchical clustering dendrograms of differentially regulated KEGG pathways predicted by PICRUSt, as described in *Materials and Methods,* from adolescent- and adult-aged male and female WT and hPXR-TG FVB/NJ mice (*t-test*, $p < 0.05$). Generated by the R packages gplots and RColorBrewer.

Supplemental Figure 10. SCFA concentrations in WT and hPXR-TG FVB/NJ mice.

Correlation plots of SCFA concentrations and differentially abundant bacteria chosen from the top 15 taxa as generated by the R packages ggplot2 and corrplot. Individual plots of significantly changed SCFAs in WT and hPXR-TG FVB/NJ mice. Asterisks represent statistically significant differences compared to WT mice (*t-test*, $p < 0.05$).

Supplemental Figure 11. Weights of WT C57BL/6J, PXR-null, CAR-null, PXR-CAR-null, WT FVB/NJ, and hPXR-TG adult mice.

Bar plots of mass (g) of adult WT C57BL/6J, PXR-null, CAR-null, PXR-CAR-null, WT FVB/NJ, and hPXR-TG male and female mice. Generated using Microsoft Excel.

Supplemental Table 1: Optimized UPLC/MS-MS gradient for bile acid chromatography

Percentages of mobile phase A (10 mM ammonium acetate with 20% acetonitrile in water) and B (10 mM ammonium acetate with 80% acetonitrile in water) per minute.

REFERENCES

Acharya A, Chan Y, Kheur S, Kheur M, Gopalakrishnan D, Watt RM, and Mattheos N (2017) Salivary microbiome of an urban Indian cohort and patterns linked to subclinical inflammation. *Oral Dis* **23:**926-940.

Ajouz H, Mukherji D, and Shamseddine A (2014) Secondary bile acids: an underrecognized cause of colon cancer. *World J Surg Oncol* **12:**164.

Aleksunes LM and Klaassen CD (2012) Coordinated regulation of hepatic phase I and II drug-metabolizing genes and transporters using AhR-, CAR-, PXR-, PPARalpha-, and Nrf2-null mice. *Drug Metab Dispos* **40:**1366-1379.

Allain T, Chaouch S, Thomas M, Travers MA, Valle I, Langella P, Grellier P, Polack B, Florent I, and Bermudez-Humaran LG (2018) Bile Salt Hydrolase Activities: A Novel Target to Screen Anti-Giardia Lactobacilli? *Front Microbiol* **9:**89.

Allain T, Chaouch S, Thomas M, Vallee I, Buret AG, Langella P, Grellier P, Polack B, Bermudez-Humaran LG, and Florent I (2017) Bile-Salt-Hydrolases from the Probiotic Strain Lactobacillus johnsonii La1 Mediate Anti-giardial Activity in Vitro and in Vivo. *Front Microbiol* **8:**2707.

Alteber Z, Sharbi-Yunger A, Pevsner-Fischer M, Blat D, Roitman L, Tzehoval E, Elinav E, and Eisenbach L (2018) The anti-inflammatory IFITM genes ameliorate colitis and partially protect from tumorigenesis by changing immunity and microbiota. *Immunol Cell Biol* **96:**284-297.

Banerjee M, Robbins D, and Chen T (2015) Targeting xenobiotic receptors PXR and CAR in human diseases. *Drug Discov Today* **20:**618-628.

Baxter NT, Schmidt AW, Venkataraman A, Kim KS, Waldron C, and Schmidt TM (2019) Dynamics of Human Gut Microbiota and Short-Chain Fatty Acids in Response to Dietary Interventions with Three Fermentable Fibers. *MBio* **10**.

Bhutia YD, Ogura J, Sivaprakasam S, and Ganapathy V (2017) Gut Microbiome and Colon Cancer: Role of Bacterial Metabolites and Their Molecular Targets in the Host. *Curr Colorectal Cancer Rep* **13:**111-118.

Bradford BU, Lock EF, Kosyk O, Kim S, Uehara T, Harbourt D, DeSimone M, Threadgill DW, Tryndyak V, Pogribny IP, Bleyle L, Koop DR, and Rusyn I (2011) Interstrain differences

in the liver effects of trichloroethylene in a multistrain panel of inbred mice. *Toxicol Sci* **120:**206-217.

Brown K, DeCoffe D, Molcan E, and Gibson DL (2012) Diet-induced dysbiosis of the intestinal microbiota and the effects on immunity and disease. *Nutrients* **4:**1095-1119.

Caparros-Martin JA, Lareu RR, Ramsay JP, Peplies J, Reen FJ, Headlam HA, Ward NC, Croft KD, Newsholme P, Hughes JD, and O'Gara F (2017) Statin therapy causes gut dysbiosis in mice through a PXR-dependent mechanism. *Microbiome* **5:**95.

Caporaso JG, Kuczynski J, Stombaugh J, Bittinger K, Bushman FD, Costello EK, Fierer N, Pena AG, Goodrich JK, Gordon JI, Huttley GA, Kelley ST, Knights D, Koenig JE, Ley RE, Lozupone CA, McDonald D, Muegge BD, Pirrung M, Reeder J, Sevinsky JR, Turnbaugh PJ, Walters WA, Widmann J, Yatsunenko T, Zaneveld J, and Knight R (2010) QIIME allows analysis of high-throughput community sequencing data. *Nat Methods* **7:**335-336.

Castro-Mejia J, Jakesevic M, Krych L, Nielsen DS, Hansen LH, Sondergaard BC, Kvist PH, Hansen AK, and Holm TL (2016) Treatment with a Monoclonal Anti-IL-12p40 Antibody Induces Substantial Gut Microbiota Changes in an Experimental Colitis Model. *Gastroenterol Res Pract* **2016:**4953120.

Chae JP, Valeriano VD, Kim GB, and Kang DK (2013) Molecular cloning, characterization and comparison of bile salt hydrolases from Lactobacillus johnsonii PF01. *J Appl Microbiol* **114:**121-133.

Chen M, Liao Z, Lu B, Wang M, Lin L, Zhang S, Li Y, Liu D, Liao Q, and Xie Z (2018) Huang-Lian-Jie-Du-Decoction Ameliorates Hyperglycemia and Insulin Resistant in Association With Gut Microbiota Modulation. *Front Microbiol* **9:**2380.

Cheng J, Krausz KW, Tanaka N, and Gonzalez FJ (2012) Chronic exposure to rifaximin causes hepatic steatosis in pregnane X receptor-humanized mice. *Toxicol Sci* **129:**456-468.

Cheng SL, Li X, Lehmler HJ, Phillips B, Shen D, and Cui JY (2018) Gut Microbiota Modulates Interactions Between Polychlorinated Biphenyls and Bile Acid Homeostasis. *Toxicol Sci* **166:**269-287.

Chiang J. Y. (2013). Bile acid metabolism and signaling. *Comprehensive Physiology*, *3*(3), 1191–1212.

Cresci GA and Bawden E (2015) Gut Microbiome: What We Do and Don't Know. *Nutr Clin Pract* **30:**734-746.

de Boussac H, Gondeau C, Briolotti P, Duret C, Treindl F, Romer M, Fabre JM, Herrero A, Ramos J, Maurel P, Templin M, Gerbal-Chaloin S, and Daujat-Chavanieu M (2018) Epidermal Growth Factor Represses Constitutive Androstane Receptor Expression in Primary Human Hepatocytes and Favors Regulation by Pregnane X Receptor. *Drug Metab Dispos* **46:**223-236.

De Smet I, Van Hoorde L, Vande Woestyne M, Christiaens H, and Verstraete W (1995) Significance of bile salt hydrolytic activities of lactobacilli. *J Appl Bacteriol* **79:**292-301.

Dempsey JL, Wang D, Siginir G, Fei Q, Raftery D, Gu H, and Yue Cui J (2019) Pharmacological Activation of PXR and CAR Downregulates Distinct Bile Acid-Metabolizing Intestinal Bacteria and Alters Bile Acid Homeostasis. *Toxicol Sci* **168:**40-60.

Deshmane SL, Kremlev S, Amini S, and Sawaya BE (2009) Monocyte chemoattractant protein-1 (MCP-1): an overview. *J Interferon Cytokine Res* **29:**313-326.

Dou W, Zhang J, Li H, Kortagere S, Sun K, Ding L, Ren G, Wang Z, and Mani S (2014) Plant flavonol isorhamnetin attenuates chemically induced inflammatory bowel disease via a PXR-dependent pathway. *J Nutr Biochem* **25:**923-933.

Dunican EM and Fahy JV (2015) The Role of Type 2 Inflammation in the Pathogenesis of Asthma Exacerbations. *Ann Am Thorac Soc* **12 Suppl 2:**S144-149.

Elcombe CR, Peffer RC, Wolf DC, Bailey J, Bars R, Bell D, Cattley RC, Ferguson SS, Geter D, Goetz A, Goodman JI, Hester S, Jacobs A, Omiecinski CJ, Schoeny R, Xie W, and Lake

BG (2014) Mode of action and human relevance analysis for nuclear receptor-mediated liver toxicity: A case study with phenobarbital as a model constitutive androstane receptor (CAR) activator. *Crit Rev Toxicol* **44:**64-82.

Elinav E, Strowig T, Kau AL, Henao-Mejia J, Thaiss CA, Booth CJ, Peaper DR, Bertin J, Eisenbarth SC, Gordon JI, and Flavell RA (2011) NLRP6 inflammasome regulates colonic microbial ecology and risk for colitis. *Cell* **145:**745-757.

Erridge C, Moncayo-Nieto OL, Morgan R, Young M, and Poxton IR (2007) Acinetobacter baumannii lipopolysaccharides are potent stimulators of human monocyte activation via Toll-like receptor 4 signalling. *J Med Microbiol* **56:**165-171.

Foley MH, O'Flaherty S, Barrangou R, and Theriot CM (2019) Bile salt hydrolases: Gatekeepers of bile acid metabolism and host-microbiome crosstalk in the gastrointestinal tract. *PLoS Pathog* **15:**e1007581.

Fu ZD, Selwyn FP, Cui JY, and Klaassen CD (2017) RNA-Seq Profiling of Intestinal Expression of Xenobiotic Processing Genes in Germ-Free Mice. *Drug Metab Dispos* **45:**1225-1238.

Gagnon L, Leduc M, Thibodeau JF, Zhang MZ, Grouix B, Sarra-Bournet F, Gagnon W, Hince K, Tremblay M, Geerts L, Kennedy CRJ, Hebert RL, Gutsol A, Holterman CE, Kamto E, Gervais L, Ouboudinar J, Richard J, Felton A, Laverdure A, Simard JC, Letourneau S, Cloutier MP, Leblond FA, Abbott SD, Penney C, Duceppe JS, Zacharie B, Dupuis J, Calderone A, Nguyen QT, Harris RC, and Laurin P (2018) A Newly Discovered Antifibrotic Pathway Regulated by Two Fatty Acid Receptors: GPR40 and GPR84. *Am J Pathol* **188:**1132-1148.

Gao J, He J, Zhai Y, Wada T, and Xie W (2009) The constitutive androstane receptor is an anti-obesity nuclear receptor that improves insulin sensitivity. *J Biol Chem* **284:**25984-25992.

Garcia-Mazcorro JF, Mills D, and Noratto G (2016) Molecular exploration of fecal microbiome in quinoa-supplemented obese mice. *FEMS Microbiol Ecol* **92**.

Golinska E, Tomusiak A, Gosiewski T, Wiecek G, Machul A, Mikolajczyk D, Bulanda M, Heczko PB, and Strus M (2013) Virulence factors of Enterococcus strains isolated from patients with inflammatory bowel disease. *World J Gastroenterol* **19:**3562-3572.

Gomes, R. N., Teixeira-Cunha, M. G., Figueiredo, R. T., Almeida, P. E., Alves, S. C., Bozza, P. T., Castro-Faria-Neto, H. C. (2013). Bacterial clearance in septic mice is modulated by MCP-1/CCL2 and nitric oxide. *Shock (Augusta, Ga.)*, *39*(1), 63–69.

Granado-Serrano AB, Martin-Gari M, Sanchez V, Riart Solans M, Berdun R, Ludwig IA, Rubio L, Vilaprinyo E, Portero-Otin M, and Serrano JCE (2019) Faecal bacterial and short-chain fatty acids signature in hypercholesterolemia. *Sci Rep* **9:**1772.

He J, Gao J, Xu M, Ren S, Stefanovic-Racic M, O'Doherty RM, and Xie W (2013) PXR ablation alleviates diet-induced and genetic obesity and insulin resistance in mice. *Diabetes* **62:**1876-1887.

Ihunnah CA, Jiang M, and Xie W (2011) Nuclear receptor PXR, transcriptional circuits and metabolic relevance. *Biochim Biophys Acta* **1812:**956-963.

Iskandar CF, Borges F, Taminiau B, Daube G, Zagorec M, Remenant B, Leisner JJ, Hansen MA, Sorensen SJ, Mangavel C, Cailliez-Grimal C, and Revol-Junelles AM (2017) Comparative Genomic Analysis Reveals Ecological Differentiation in the Genus Carnobacterium. *Front Microbiol* **8:**357.

Jackson MA, Jeffery IB, Beaumont M, Bell JT, Clark AG, Ley RE, O'Toole PW, Spector TD, and Steves CJ (2016) Signatures of early frailty in the gut microbiota. *Genome Med* **8:**8.

Jena PK, Sheng L, Liu HX, Kalanetra KM, Mirsoian A, Murphy WJ, French SW, Krishnan VV, Mills DA, and Wan YY (2017) Western Diet-Induced Dysbiosis in Farnesoid X Receptor Knockout Mice Causes Persistent Hepatic Inflammation after Antibiotic Treatment. *Am J Pathol* **187:**1800-1813.

Jiang Y, Feng D, Ma X, Fan S, Gao Y, Fu K, Wang Y, Sun J, Yao X, Liu C, Zhang H, Xu L, Liu A, Gonzalez FJ, Yang Y, Gao B, Huang M, and Bi H (2019) Pregnane X Receptor Regulates Liver Size and Liver Cell Fate by Yes-Associated Protein Activation in Mice. *Hepatology* **69:**343-358.

Jun SH, Lee JH, Kim BR, Kim SI, Park TI, Lee JC, and Lee YC (2013) Acinetobacter baumannii outer membrane vesicles elicit a potent innate immune response via membrane proteins. *PLoS One* **8:**e71751.

Kikuchi-Ueda T, Kamoshida G, Ubagai T, Nakano R, Nakano A, Akuta T, Hikosaka K, Tansho-Nagakawa S, Kikuchi H, and Ono Y (2017) The TNF-alpha of mast cells induces pro-inflammatory responses during infection with Acinetobacter baumannii. *Immunobiology* **222:**1025-1034.

Kim CH, Park J, and Kim M (2014) Gut microbiota-derived short-chain Fatty acids, T cells, and inflammation. *Immune Netw* **14:**277-288.

Kublbeck J, Zancanella V, Prantner V, Molnar F, Squires EJ, Dacasto M, Honkakoski P, and Giantin M (2016) Characterization of ligand-dependent activation of bovine and pig constitutive androstane (CAR) and pregnane X receptors (PXR) with interspecies comparisons. *Xenobiotica* **46:**200-210.

Kumar RS, Brannigan JA, Prabhune AA, Pundle AV, Dodson GG, Dodson EJ, and Suresh CG (2006) Structural and functional analysis of a conjugated bile salt hydrolase from Bifidobacterium longum reveals an evolutionary relationship with penicillin V acylase. *J Biol Chem* **281:**32516-32525.

Lai ZL, Tseng CH, Ho HJ, Cheung CKY, Lin JY, Chen YJ, Cheng FC, Hsu YC, Lin JT, El-Omar EM, and Wu CY (2018) Fecal microbiota transplantation confers beneficial metabolic effects of diet and exercise on diet-induced obese mice. *Sci Rep* **8:**15625.

Larsen JM (2017) The immune response to Prevotella bacteria in chronic inflammatory disease. *Immunology* **151:**363-374.

LeCluyse EL (2001) Pregnane X receptor: molecular basis for species differences in CYP3A induction by xenobiotics. *Chem Biol Interact* **134:**283-289.

Li CY, Dempsey JL, Wang D, Lee S, Weigel KM, Fei Q, Bhatt DK, Prasad B, Raftery D, Gu H, and Cui JY (2018) PBDEs Altered Gut Microbiome and Bile Acid Homeostasis in Male C57BL/6J Mice. *Drug Metab Dispos* **46:**1226-1240.

Li CY, Lee S, Cade S, Kuo LJ, Schultz IR, Bhatt DK, Prasad B, Bammler TK, and Cui JY (2017a) Novel Interactions between Gut Microbiome and Host Drug-Processing Genes Modify the Hepatic Metabolism of the Environmental Chemicals Polybrominated Diphenyl Ethers. *Drug Metab Dispos* **45:**1197-1214.

Li Q, Lauber CL, Czarnecki-Maulden G, Pan Y, and Hannah SS (2017b) Effects of the Dietary Protein and Carbohydrate Ratio on Gut Microbiomes in Dogs of Different Body Conditions. *MBio* **8**.

Li T and Apte U (2015) Bile Acid Metabolism and Signaling in Cholestasis, Inflammation, and Cancer. *Adv Pharmacol* **74:**263-302.

Li Z, Wright AD, Liu H, Bao K, Zhang T, Wang K, Cui X, Yang F, Zhang Z, and Li G (2015) Bacterial community composition and fermentation patterns in the rumen of sika deer (Cervus nippon) fed three different diets. *Microb Ecol* **69:**307-318.

Lindenbaum J, Rund DG, Butler VP, Jr., Tse-Eng D, and Saha JR (1981) Inactivation of digoxin by the gut flora: reversal by antibiotic therapy. *N Engl J Med* **305:**789-794.

Luca F, Kupfer SS, Knights D, Khoruts A, and Blekhman R (2018) Functional Genomics of Host-Microbiome Interactions in Humans. *Trends Genet* **34:**30-40.

Luerce TD, Gomes-Santos AC, Rocha CS, Moreira TG, Cruz DN, Lemos L, Sousa AL, Pereira VB, de Azevedo M, Moraes K, Cara DC, LeBlanc JG, Azevedo V, Faria AMC, and Miyoshi A (2014) Anti-inflammatory effects of Lactococcus lactis NCDO 2118 during the remission period of chemically induced colitis. *Gut Pathog* **6:**33.

Ma N, Guo P, Zhang J, He T, Kim SW, Zhang G, and Ma X (2018) Nutrients Mediate Intestinal Bacteria-Mucosal Immune Crosstalk. *Front Immunol* **9:**5.

Martinez KB, Pierre JF, and Chang EB (2016) The Gut Microbiota: The Gateway to Improved Metabolism. *Gastroenterol Clin North Am* **45:**601-614.

Meneses ME, Martinez-Carrera D, Torres N, Sanchez-Tapia M, Aguilar-Lopez M, Morales P, Sobal M, Bernabe T, Escudero H, Granados-Portillo O, and Tovar AR (2016) Hypocholesterolemic Properties and Prebiotic Effects of Mexican Ganoderma lucidum in C57BL/6J Mice. *PLoS One* **11:**e0159631.

Miyoshi J, Nobutani K, Musch MW, Ringus DL, Hubert NA, Yamamoto M, Kase Y, Nishiyama M, and Chang EB (2018) Time-, Sex-, and Dose-Dependent Alterations of the Gut Microbiota by Consumption of Dietary Daikenchuto (TU-100). *Evid Based Complement Alternat Med* **2018:**7415975.

Mutoh S, Sobhany M, Moore R, Perera L, Pedersen L, Sueyoshi T, and Negishi M (2013) Phenobarbital indirectly activates the constitutive active androstane receptor (CAR) by inhibition of epidermal growth factor receptor signaling. *Sci Signal* **6:**ra31.

O'Flaherty S, Briner Crawley A, Theriot CM, and Barrangou R (2018) The Lactobacillus Bile Salt Hydrolase Repertoire Reveals Niche-Specific Adaptation. *mSphere* **3**.

Ohbuchi M, Yoshinari K, Kaneko H, Matsumoto S, Inoue A, Kawamura A, Usui T, and Yamazoe Y (2013) Coordinated roles of pregnane X receptor and constitutive androstane receptor in autoinduction of voriconazole metabolism in mice. *Antimicrob Agents Chemother* **57:**1332-1338.

Oladimeji PO and Chen T (2018) PXR: More Than Just a Master Xenobiotic Receptor. *Mol Pharmacol* **93:**119-127.

Olbjorn C, Cvancarova Smastuen M, Thiis-Evensen E, Nakstad B, Vatn MH, Jahnsen J, Ricanek P, Vatn S, Moen AEF, Tannaes TM, Lindstrom JC, Soderholm JD, Halfvarson J, Gomollon F, Casen C, Karlsson MK, Kalla R, Adams AT, Satsangi J, and Perminow G

(2019) Fecal microbiota profiles in treatment-naive pediatric inflammatory bowel disease - associations with disease phenotype, treatment, and outcome. *Clin Exp Gastroenterol* **12:**37-49.

Pallister T, Jackson MA, Martin TC, Glastonbury CA, Jennings A, Beaumont M, Mohney RP, Small KS, MacGregor A, Steves CJ, Cassidy A, Spector TD, Menni C, and Valdes AM (2017) Untangling the relationship between diet and visceral fat mass through blood metabolomics and gut microbiome profiling. *Int J Obes (Lond)* **41:**1106-1113.

Park S, Cheng SL, and Cui JY (2016) Characterizing drug-metabolizing enzymes and transporters that are bona fide CAR-target genes in mouse intestine. *Acta Pharm Sin B* **6:**475-491.

Pencikova K, Svrzkova L, Strapacova S, Neca J, Bartonkova I, Dvorak Z, Hyzdalova M, Pivnicka J, Palkova L, Lehmler HJ, Li X, Vondracek J, and Machala M (2018) In vitro profiling of toxic effects of prominent environmental lower-chlorinated PCB congeners linked with endocrine disruption and tumor promotion. *Environ Pollut* **237:**473-486.

Png CW, Linden SK, Gilshenan KS, Zoetendal EG, McSweeney CS, Sly LI, McGuckin MA, and Florin TH (2010) Mucolytic bacteria with increased prevalence in IBD mucosa augment in vitro utilization of mucin by other bacteria. *Am J Gastroenterol* **105:**2420-2428.

Qiu Z, Cervantes JL, Cicek BB, Mukherjee S, Venkatesh M, Maher LA, Salazar JC, Mani S, and Khanna KM (2016) Pregnane X Receptor Regulates Pathogen-Induced Inflammation and Host Defense against an Intracellular Bacterial Infection through Toll-like Receptor 4. *Sci Rep* **6:**31936.

Rahim SS, Khan N, Boddupalli CS, Hasnain SE, and Mukhopadhyay S (2005) Interleukin-10 (IL-10) mediated suppression of IL-12 production in RAW 264.7 cells also involves c-rel transcription factor. *Immunology* **114:**313-321.

Ranhotra HS, Flannigan KL, Brave M, Mukherjee S, Lukin DJ, Hirota SA, and Mani S (2016) Xenobiotic Receptor-Mediated Regulation of Intestinal Barrier Function and Innate Immunity. *Nucl Receptor Res* **3**.

Reunanen J, Kainulainen V, Huuskonen L, Ottman N, Belzer C, Huhtinen H, de Vos WM, and Satokari R (2015) Akkermansia muciniphila Adheres to Enterocytes and Strengthens the Integrity of the Epithelial Cell Layer. *Appl Environ Microbiol* **81:**3655-3662.

Ridlon JM, Harris SC, Bhowmik S, Kang DJ, and Hylemon PB (2016) Consequences of bile salt biotransformations by intestinal bacteria. *Gut Microbes* **7:**22-39.

Ridlon JM, Kang DJ, and Hylemon PB (2006) Bile salt biotransformations by human intestinal bacteria. *J Lipid Res* **47:**241-259.

Ridlon JM, Kang DJ, Hylemon PB, and Bajaj JS (2014) Bile acids and the gut microbiome. *Curr Opin Gastroenterol* **30:**332-338.

Ring C, Klopfleisch R, Dahlke K, Basic M, Bleich A, and Blaut M (2019) Akkermansia muciniphila strain ATCC BAA-835 does not promote short-term intestinal inflammation in gnotobiotic interleukin-10-deficient mice. *Gut Microbes* **10:**188-203.

Riviere A, Selak M, Lantin D, Leroy F, and De Vuyst L (2016) Bifidobacteria and Butyrate-Producing Colon Bacteria: Importance and Strategies for Their Stimulation in the Human Gut. *Front Microbiol* **7:**979.

Scarpignato C, Dolak W, Lanas A, Matzneller P, Renzulli C, Grimaldi M, Zeitlinger M, and Bjarnason I (2017) Rifaximin Reduces the Number and Severity of Intestinal Lesions Associated With Use of Nonsteroidal Anti-Inflammatory Drugs in Humans. *Gastroenterology* **152:**980-982 e983.

Seekatz AM, Schnizlein MK, Koenigsknecht MJ, Baker JR, Hasler WL, Bleske BE, Young VB, and Sun D (2019) Spatial and Temporal Analysis of the Stomach and Small-Intestinal Microbiota in Fasted Healthy Humans. *mSphere* **4**.

Selwyn FP, Cheng SL, Bammler TK, Prasad B, Vrana M, Klaassen C, and Cui JY (2015) Developmental Regulation of Drug-Processing Genes in Livers of Germ-Free Mice. *Toxicol Sci* **147:**84-103.

Sender R, Fuchs S, and Milo R (2016) Are We Really Vastly Outnumbered? Revisiting the Ratio of Bacterial to Host Cells in Humans. *Cell* **164:**337-340.

Shah YM, Ma X, Morimura K, Kim I, and Gonzalez FJ (2007) Pregnane X receptor activation ameliorates DSS-induced inflammatory bowel disease via inhibition of NF-kappaB target gene expression. *Am J Physiol Gastrointest Liver Physiol* **292:**G1114-1122.

Shimizu J, Kubota T, Takada E, Takai K, Fujiwara N, Arimitsu N, Murayama MA, Ueda Y, Wakisaka S, Suzuki T, and Suzuki N (2018) Propionate-producing bacteria in the intestine may associate with skewed responses of IL10-producing regulatory T cells in patients with relapsing polychondritis. *PLoS One* **13:**e0203657.

Sivaprakasam S, Bhutia YD, Ramachandran S, and Ganapathy V (2017) Cell-Surface and Nuclear Receptors in the Colon as Targets for Bacterial Metabolites and Its Relevance to Colon Health. *Nutrients* **9**.

Smith PM, Howitt MR, Panikov N, Michaud M, Gallini CA, Bohlooly YM, Glickman JN, and Garrett WS (2013) The microbial metabolites, short-chain fatty acids, regulate colonic Treg cell homeostasis. *Science* **341:**569-573.

Staudinger JL, Goodwin B, Jones SA, Hawkins-Brown D, MacKenzie KI, LaTour A, Liu Y, Klaassen CD, Brown KK, Reinhard J, Willson TM, Koller BH, and Kliewer SA (2001) The nuclear receptor PXR is a lithocholic acid sensor that protects against liver toxicity. *Proc Natl Acad Sci U S A* **98:**3369-3374.

Toda T, Saito N, Ikarashi N, Ito K, Yamamoto M, Ishige A, Watanabe K, and Sugiyama K (2009) Intestinal flora induces the expression of Cyp3a in the mouse liver. *Xenobiotica* **39:**323-334.

Turnbaugh PJ, Backhed F, Fulton L, and Gordon JI (2008) Diet-induced obesity is linked to marked but reversible alterations in the mouse distal gut microbiome. *Cell Host Microbe* **3:**213-223.

Turnbaugh PJ, Ridaura VK, Faith JJ, Rey FE, Knight R, and Gordon JI (2009) The effect of diet on the human gut microbiome: a metagenomic analysis in humanized gnotobiotic mice. *Sci Transl Med* **1:**6ra14.

Ueda A, Hamadeh HK, Webb HK, Yamamoto Y, Sueyoshi T, Afshari CA, Lehmann JM, and Negishi M (2002) Diverse roles of the nuclear orphan receptor CAR in regulating hepatic genes in response to phenobarbital. *Mol Pharmacol* **61:**1-6.

Venkatesh M, Mukherjee S, Wang H, Li H, Sun K, Benechet AP, Qiu Z, Maher L, Redinbo MR, Phillips RS, Fleet JC, Kortagere S, Mukherjee P, Fasano A, Le Ven J, Nicholson JK, Dumas ME, Khanna KM, and Mani S (2014) Symbiotic bacterial metabolites regulate gastrointestinal barrier function via the xenobiotic sensor PXR and Toll-like receptor 4. *Immunity* **41:**296-310.

Wang Y, Xiang X, Huang WW, Sandford AJ, Wu SQ, Zhang MM, Wang MG, Chen G, and He JQ (2019) Association of PXR and CAR Polymorphisms and Antituberculosis Drug-Induced Hepatotoxicity. *Sci Rep* **9:**2217.

Watanabe M, Houten SM, Mataki C, Christoffolete MA, Kim BW, Sato H, Messaddeq N, Harney JW, Ezaki O, Kodama T, Schoonjans K, Bianco AC, and Auwerx J (2006) Bile acids induce energy expenditure by promoting intracellular thyroid hormone activation. *Nature* **439:**484-489.

Watkins RE, Wisely GB, Moore LB, Collins JL, Lambert MH, Williams SP, Willson TM, Kliewer SA, and Redinbo MR (2001) The human nuclear xenobiotic receptor PXR: structural determinants of directed promiscuity. *Science* **292:**2329-2333.

Whitfield-Cargile CM, Cohen ND, Chapkin RS, Weeks BR, Davidson LA, Goldsby JS, Hunt CL, Steinmeyer SH, Menon R, Suchodolski JS, Jayaraman A, and Alaniz RC (2016) The

microbiota-derived metabolite indole decreases mucosal inflammation and injury in a murine model of NSAID enteropathy. *Gut Microbes* **7:**246-261.

Williams BL, Hornig M, Parekh T, and Lipkin WI (2012) Application of novel PCR-based methods for detection, quantitation, and phylogenetic characterization of Sutterella species in intestinal biopsy samples from children with autism and gastrointestinal disturbances. *MBio* **3**.

Wong K, Bumpstead S, Van Der Weyden L, Reinholdt LG, Wilming LG, Adams DJ, and Keane TM (2012) Sequencing and characterization of the FVB/NJ mouse genome. *Genome Biol* **13:**R72.

Wu GD, Chen J, Hoffmann C, Bittinger K, Chen YY, Keilbaugh SA, Bewtra M, Knights D, Walters WA, Knight R, Sinha R, Gilroy E, Gupta K, Baldassano R, Nessel L, Li H, Bushman FD, and Lewis JD (2011) Linking long-term dietary patterns with gut microbial enterotypes. *Science* **334:**105-108.

Wu W, Lv L, Shi D, Ye J, Fang D, Guo F, Li Y, He X, and Li L (2017) Protective Effect of Akkermansia muciniphila against Immune-Mediated Liver Injury in a Mouse Model. *Front Microbiol* **8:**1804.

Xu C, Huang M, and Bi H (2016) PXR- and CAR-mediated herbal effect on human diseases. *Biochim Biophys Acta* **1859:**1121-1129.

Yun Y, Kim HN, Kim SE, Heo SG, Chang Y, Ryu S, Shin H, and Kim HL (2017) Comparative analysis of gut microbiota associated with body mass index in a large Korean cohort. *BMC Microbiol* **17:**151.

Zhang YK, Lu H, and Klaassen CD (2013) Expression of human CAR splicing variants in BAC-transgenic mice. *Toxicol Sci* **132:**142-150.

Zhao S, Liu W, Wang J, Shi J, Sun Y, Wang W, Ning G, Liu R, and Hong J (2017) Akkermansia muciniphila improves metabolic profiles by reducing inflammation in chow diet-fed mice. *J Mol Endocrinol* **58:**1-14.

Zhou H and Hylemon PB (2014) Bile acids are nutrient signaling hormones. *Steroids* **86:**62-68.